Modelling of sand-mud mixtures

Part II: A process-based sand-mud model

Mathijs van Ledden

January, 2001

Contents

List of Figures

List of Tables

1 Introduction 1–1

1.1 Sand-mud segregation 1–1

1.2 Problem definition 1–2

1.3 Objectives 1–4

1.4 Outline 1–5

1.5 Project organisation 1–5

2 Model formulations 2–1

2.1 Introduction 2–1

2.2 Flow model 2–2

2.3 Sediment transport model 2–4

2.3.1 General 2–4
2.3.2 Suspended sediment transport 2–5
2.3.3 Bed load transport 2–11

2.4 Bed model 2–12

2.4.1 Bed level 2–12
2.4.2 Bed composition 2–12

3 Numerical modelling 3–1

3.1 Introduction 3–1

3.2 Modifications in DELFT3D-FLOW 3–1

3.2.1 Overview 3–1
3.2.2 Sediment transport 3–3
3.2.3 Bed level 3–5
3.2.4 Bed composition 3–6

3.3 Numerical apects 3–8

3.3.1 Flow 3–8
3.3.2 Sediment transport 3–8
3.3.3 Bed level 3–9
3.3.4 Bed composition 3–9

4 Case study: Noordelijk Deltabekken 4–1

4.1 Introduction 4–1

4.2 Sand-mud patterns 4–2

4.3 Model set-up 4–5

4.3.1 Introduction 4–5
4.3.2 Geometry 4–5
4.3.3 Boundary conditions 4–5
4.3.4 Bathymetry 4–6
4.3.5 Sediment parameters 4–7
4.3.6 Initial conditions 4–10
4.3.7 Numerical parameters 4–10

4.4 Results 4–13

4.5 Analysis 4–16

4.5.1 Sand wave 4–16
4.5.2 Mud wave 4–17

4.6 Discussion 4–22

5 Conclusions and recommendations 5–1

5.1 Conclusions 5–1

5.2 Recommendations 5–2

6 References 6–1

Appendix A Figures A-1

Appendix B Mud wave characteristics B-1

B.1 Onset of mud wave B-1
B.2 Mud concentration B-3
B.3 Maximum mud deposition B-5

List of Figures

Figure 1-1 Location (a), water depth (b) and mud content (c) Hollandsch Diep..... 1–1
Figure 1-2 Correlation between LHEC and mud content in the bed 1–3
Figure 1-3 Comparison between field data and model results..... 1–4
Figure 2-1 Morphological models at present (a) and extensions for sand-mud model (b) . 2–1
Figure 2-2 Flow variables 2–3
Figure 2-3 Sand and mud transport..... 2–5
Figure 2-4 Net suspended sand and mud flux at bed boundary 2–8
Figure 2-5 Sand-silt-clay triangle and permeability C_v..... 2–9
Figure 2-6 Definitions bed composition 2–13
Figure 2-7 Physical and biological mixing coefficient 2–15
Figure 3-1 Overview of discretisation 3–2
Figure 4-1 Noordelijk Deltabekken 4–1
Figure 4-2 Deposition (+)/Erosion (-) rates per unit area for river branches 1971-1982 ... 4–4
Figure 4-3 Deposition (+)/Erosion (-) rates per unit area for river branches 1982-1992 ... 4–4
Figure 4-4 Mud concentration along the basin 4–19
Figure 4-5 Mud deposition along the basin after five years 4–20
Figure 4-6 Length scale L_d..... 4–21
Figure 4-7 Computed bed level changes for reference computation 4–22

List of Tables

Table 3-1 Parameters in inputfile BEDCOM.inp 3–3
Table 4-1 Annual supply of sand and mud (*10^9 kg/year) 4–2
Table 4-2 Total deposition (+)/erosion (-) of sand and mud 1971-1982 4–2
Table 4-3 Annual deposition (+)/erosion (-) rate of sand and mud 1982-1992 4–3
Table 4-4 Sediment transport rates and annual load for various grain sizes 4–8
Table 4-5 Parameter values for reference computation 4–9
Table 4-6 Overview of computations 4–10
Table 4-7 Overview of computations 4–13
Table 4-8 Critical water depth and onset for mud deposition 4–18
Table 4-9 Length scales and distance of the maximum mud deposition 4–19

Summary

The sediments in many estuaries consist of non-cohesive and cohesive fractions, and the mud content in the bed (% < 63 μm) often shows strong variations in both horizontal and vertical directions. This phenomenon is called sand-mud segregation. For the sustainable management and development of these areas, the understanding of and ability to predict this segregation is highly desirable.

The present project "Modelling of sand-mud mixtures" (Z2840) is a collaboration between the research project "Zand-slib" at WL | DELFT HYDRAULICS and the Ph.D.-project "Large-scale segregation in estuaries and tidal lagoons" (STW-project DCT.4895) at Delft University of Technology. The latter project is supported by the Technology Foundation STW and also included in the Eco-morphology project within Delft Cluster.

The aim was to contribute to a better understanding and predictability of sand-mud segregation in estuaries. Recently, two modelling tools for predicting the bed level and bed composition have been developed: the semi-empirical model LHEC (Wang, 1997) and the process-based sand-mud model (Van Ledden & Wang, 2000). At present, neither approach can be considered superior to the other. Therefore, both modelling tools were further elaborated in this study. The results have been described in Part I and Part II respectively.

- **Part I: Application of LHEC[1] to Haringvliet - Hollandsch Diep**

The semi-empirical model LHEC computes the tide-averaged equilibrium concentration using the local water depth and bed shear stress as derived from the DELFT3D flow model. LHEC employs process formulations for the erosion and deposition of mud using the following mud properties: the settling velocity, the critical shear stresses for erosion and deposition and an erosion parameter. In this way the LHEC value is computed in each point of the computational grid and compared with a local measurement of the sand content of the bed. If LHEC is relatively large, also erosion is large (and deposition small) and thus a low mud content in the bed is expected. The basic assumption for the model is that in each location there is an unlimited supply of suspended sediment, i.e. if local conditions are favourable for deposition, the model predicts that a mud bed will be formed.

LHEC was applied to the Hollandsch Diep and Haringvliet, both part of the Noordelijk Deltabekken which is the estuary of the rivers Rhine and Meuse. An extensive data set on the bed composition was available giving the sand content on a rectangular 10 m grid. The computed LHEC values were compared with the local sand content by means of scatter diagrams. These scatter diagrams showed that LHEC can discriminate between sediments with a sand content less than 65% and sediments with a sand content larger than 65%. However, such a result was only found for the Hollandsch Diep upstream (east) of the location of the sedimentation front, suggesting that the sediment supply cannot be a limiting factor for reliable predictions.

[1] Acronym for **L**ocal **H**ypothetical **E**quilibrium **C**oncentration

- **Part II: A process-based sand-mud model**

Model formulations for a process-based morphological model with a sand and a mud fraction were proposed. The main extensions to the present morphological models are that the bed level changes depend on both suspended sand and mud exchange at the bed-water interface, and on bed load transport gradients of sand. Furthermore, the bed composition is time-dependent and non-uniform in horizontal and vertical direction.

The morphological behaviour of a schematic basin was analysed. This situation is qualitatively comparable with the southern area of the Noordelijk Deltabekken (The Netherlands) in which sand and mud was deposited after the construction of the Haringvliet sluices in 1970. The geometry and the boundary conditions were strongly simplified in order to determine governing length scales by an analytical approach.

The model results showed a sand deposition wave and a mud deposition wave propagating in downstream direction. The form of the mud wave strongly depends on two adaptation length scales for mud: a 'settling length scale' and a 'flow length scale'. The expression for the settling length scale is equal to the well-known adaptation length scale for suspended sand transport, but differs because of another settling velocity. The 'flow length scale' depends on both the actual bed level slope and the critical velocity for mud deposition. This length scale expresses a characteristic distance in which the (depth-averaged) flow velocity becomes two times smaller than the critical (depth-averaged) velocity for deposition.

Due to the simplified geometry and boundary conditions, the computational results could only qualitatively be compared with two sediment balances (1971-1982 and 1982-1992) for different sections in the Noordelijk Deltabekken. Various morphological characteristics, as found from the numerical computations (e.g. sand wave, mud wave, maximum mud deposition), are also observed in both, or at least one, of the sediment balances. The simplified model set-up and also the determination of the deposited sand and mud volumes in the sediment balances, result in several differences between the model results and the field data.

In particular for the Haringvliet and Hollandsch Diep, the model results suggest that the high mud deposition rate in the Hollandsch Diep area is caused by two interacting factors. On the one hand, the suspended mud concentration is relatively high due to the absence of mud deposition in the upstream areas. On the other hand, the flow velocity is relatively low, so mud deposition can occur. For the upstream river branches (Nieuwe Merwede, Boven-Merwede) the relatively low mud deposition compared with the Hollandsch Diep is mainly caused by the high flow velocities. For the downstream area (Haringvliet), the relatively low mud deposition is caused by the low mud concentration in the water column.

The model results also suggest that predicting the mud content with a local parameter is probably not very successful in areas in which the mud concentration in the water column strongly varies in horizontal direction. In addition to the local hydrodynamics, the mud supply from upstream is a very important factor in the development of the local mud content in the bed.

1 Introduction

1.1 Sand-mud segregation

In many estuaries with non-cohesive and cohesive sediments the mud content in the bed (% < 63 µm) often shows strong variations in both horizontal and vertical directions. This phenomenon is called sand-mud segregation. An example of sand-mud segregation is given in Figure 1.1 (source: Venema et al., 1998).

Figure 1-1 Location (a), water depth (b) and mud content (c) Hollandsch Diep

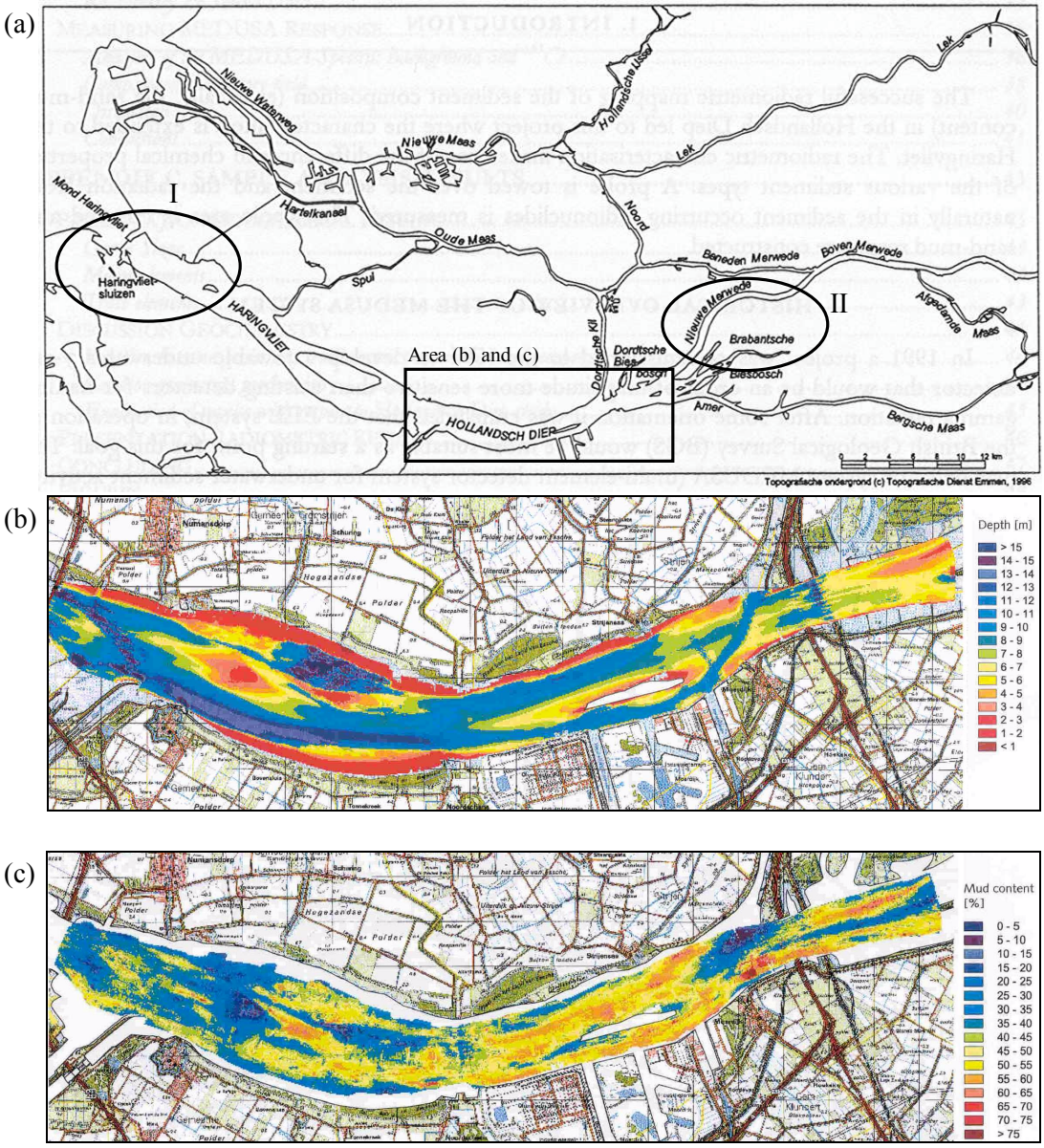

The water depth (Figure 1-1b) and the mean mud content in the upper 10 - 20 cm of the bed (Figure 1-1c) are shown for the Hollandsch Diep. This area is a section of the estuary of the River Rhine and Meuse in the western part of the Netherlands (Figure 1-1a). Mud content variations can be observed between shallow borders and deep channels, but the mud content also varies in the longitudinal direction. The mud content in the central part of the Hollandsch Diep is much higher than in the west and near the river branches Nieuwe Merwede and Amer in the east.

An understanding of and ability to predict this phenomenon is necessary for sustainable management and development of these areas, because both sand and mud determine the development of the bed level and the bed composition in time and space (i.e. morphological behaviour). In general, bed level changes affect the navigation depth and high water levels and are therefore important for the maintenance of navigation channels and the safety of the surrounding areas. Moreover, the mud content of the bed is an important parameter for the sediment bed quality, because nutrients and pollutants tend to adhere to, or be part of, cohesive sediments only.

In the aforementioned Hollandsch Diep, but also in the Haringvliet and the other river branches, an enormous amount of sand and mud was deposited after construction of the Haringvliet sluices in 1970 (indicated by I in Figure 1.1a). The present management strategy is that these sluices are only open during ebb tide. In the future the sluices will be partially open during flood tide in order to re-introduce the tide in the system. For this part of the estuary the specific research question is what the bed level and bed composition development will be after changing the management strategy.

1.2 Problem definition

Recently WL | DELFT HYDRAULICS carried out several studies for Rijkswaterstaat-RIZA with respect to the predictability of sand-mud segregation. The study area was the estuary of the River Rhine and Meuse in the western part of the Netherlands (Figure 1.1a).

Kuijper (1995a) described sand-mud patterns in sediment bed cores and bed samples from the river branch Nieuwe Merwede (indicated by II in Figure 1.1a). Van den Boogaard & Kuijper (1995) presented several statistical methods to identify sand-mud patterns by using cores and bed samples. However, these methods were not applied to the study area due to lack of data. Kuijper (1995b) gave an overview of erosion experiments with sand-mud mixtures and described the effect of mud on sand properties and vice versa.

Wang (1996) presented several options for predicting the bed composition, varying from a fully data-based approach to a fully process-based approach. It was decided that a combination of process and empirical knowledge (i.e. semi-empirical approach) is at present the most promising way for predicting the mud content. A semi-empirical model (LHEC) was proposed, which was further developed and tested against field data from the Nieuwe Merwede (indicated by II in Figure 1.1a), a river branch with only a small tidal influence (Wang, 1997). It was concluded that LHEC could distinguish areas with a mud

content lower than about 10% and areas with a mud content between 0 and 100% (Figure 1-2).

Figure 1-2 Correlation between LHEC and mud content in the bed

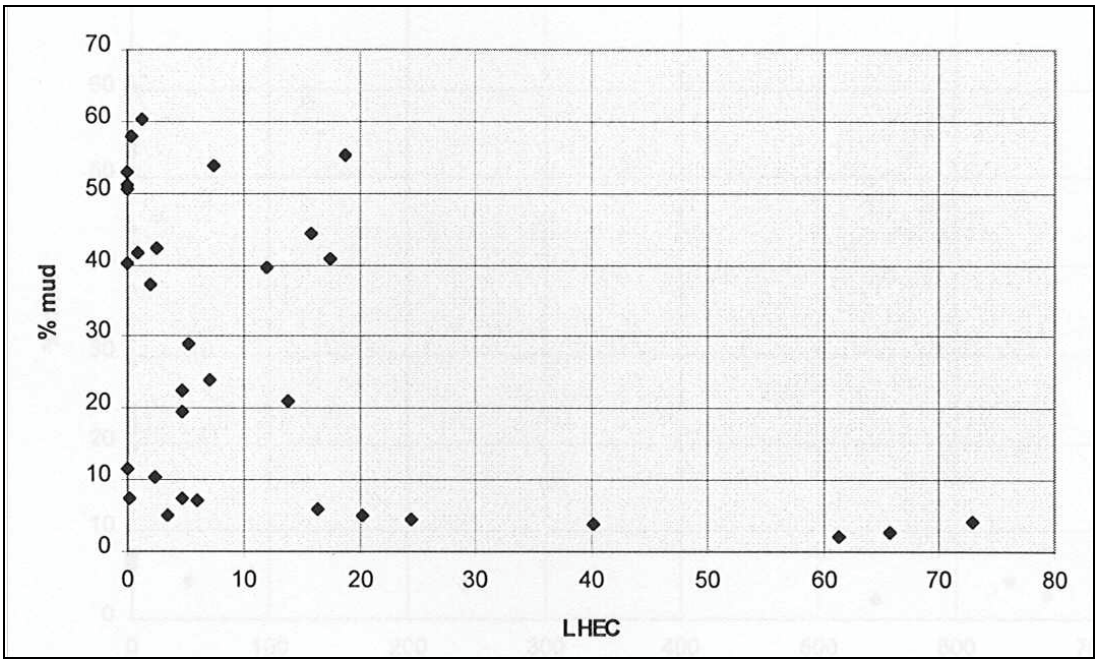

However, the Nieuwe Merwede has strong river characteristics. A question arising from this study includes whether this distinction is also found for an estuarine environment in which the tide and/or wind waves are more important.

Several other studies are also worth mentioning with respect to sand-mud segregation. Venema et al. (1998) showed that the sand-mud ratio in underwater surface sediment can be obtained by measuring the radiometric characteristics This technique is based on differences in concentrations of (natural) radionuclides in various sediment components. This technique was applied to the Hollandsch Diep (Venema et al., 1999) and Haringvliet (Venema et al., 2000) and very detailed sand-mud maps were obtained. This extensive data-set can be very useful for further developing and validation of the aforementioned LHEC, since the tide and wind waves are important for the hydrodynamic forcing in this area.

Van Ledden (2000) gave an overview of the present knowledge with respect to sand-mud segregation in estuaries and tidal lagoons. Field measurements, the mechanisms behind sand-mud segregation, predictive models, and laboratory experiments were discussed. An important conclusion was that a process-based sand-mud model does not presently exist.

Van Ledden & Wang (2000) proposed formulations for a process-based model for sand and mud in which horizontal and vertical mud content variations in the bed were included. These formulations were only used to analyse vertical mud content variations in the bed. Furthermore, the so-called ‘local approach’ was carried out for a schematic tidal situation (constant water depth, symmetric tidal current). The analysis showed that an equilibrium mud content in the bed can be found. It depends on the local hydrodynamics, the local mud concentration in the water column, the settling velocity, the erosion rate and the critical

shear stresses for erosion and deposition. Compared with field data the equilibrium mud content appears to be the upper limit for the mud content in a certain area (Figure 1-3).

Figure 1-3 Comparison between field data and model results

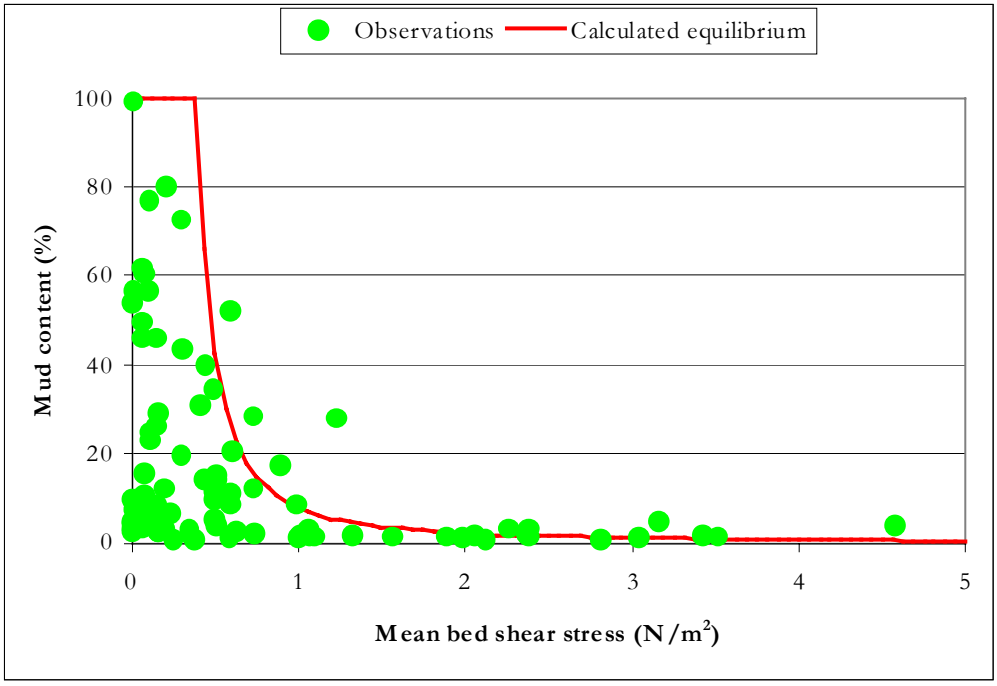

The next step is to build a process-based morphological model with these sand-mud formulations in which horizontal variations in the mud content in the bed are also included.

1.3 Objectives

The aim is to contribute to a better understanding and predictability of sand-mud segregation in estuaries. Two modelling tools for predicting the bed composition are described in section 1.2: the semi-empirical model (LHEC) and a process-based sand-mud model. The research questions associated with both approaches were discussed previously.

At present, neither approach can be considered superior to the other. Although the process-based approach incorporates much more physical knowledge, prediction of long-term bed level and bed composition changes are still not feasible. Therefore, both modelling approaches are being further elaborated in this study.

A large data-set of mud content measurements was obtained for the Haringvliet and Hollandsch Diep (Venema et al., 1999; Venema et al., 2000). Because wind waves and tide are important for the hydrodynamic forcing in this area, LHEC is further developed and validated in one part of the project, using this data-set. The results are presented in Part I: Application of LHEC to Haringvliet - Hollandsch Diep.

Furthermore, a process-based morphological model is developed in which both horizontal and vertical mud content variations in the bed are included. With such a model, both horizontal and vertical mud content variations in the bed can be analysed. This process-based approach is described in the present part of the report (Part II: A process-based sand-mud model).

1.4 Outline

In Chapter 2, the background of the model formulations used are discussed. The implementation of these model formulations in a numerical model are described in Chapter 3. In Chapter 4 the morphological model is applied for a schematic estuary with both sand and mud supply in which the tide is eliminated due to a man-made structure. Finally, conclusions and recommendations are given in Chapter 5.

1.5 Project organisation

The present project "Modelling of sand-mud mixtures" (Z2840) is a collaboration between the research project "Zand-slib" at WL | DELFT HYDRAULICS and the Ph.D.-project "Large-scale segregation in estuaries and tidal lagoons" (DCT.4895) at Delft University of Technology. The research project "Zand-slib is funded by "Doelsubsidie" (Ministry of Transport and Public Works). The Ph.D. project is supported by STW, applied science division of NWO and the technology programme of the Ministry of Economic Affairs and is also included in the Eco-morphology project within Delft Cluster.

Part I of the study (*Application of LHEC to Haringvliet - Hollandsch Diep*) was carried out by R. Bruinsma (software development, data processing and hydrodynamic runs) and C. Kuijper (LHEC application and reporting[2]). Part II (*A process-based sand-mud model*) was executed by M. van Ledden of Delft University of Technology and supervised by dr. Z.B. Wang. The work of Van Ledden forms part of his PhD-dissertation.

[2] *Chapter 1 of report I was written by M. van Ledden and is also included in Part II.*

2 Model formulations

2.1 Introduction

Morphological behaviour is the dynamic interaction between hydrodynamics, due to waves and currents, and the bed level and composition. The crucial link between the hydrodynamics and the bed is formed by the transport of various sediment fractions. The behaviour is called dynamic because of the feedback from changes in bed level and bed composition on the hydrodynamics.

At present, morphological models only exist for non-cohesive sediments. For cohesive sediments the feedback between the bed level changes and the hydrodynamics is not taken into account. The main assumptions in existing morphological models are:

- water motion is not affected by the suspended sediment concentrations;
- a uniform and time-independent bed roughness parameter;
- one representative non-cohesive sediment fraction;
- uniform and time-independent bed composition;

These models consist of three sub-models in which the hydrodynamics, sediment transport and bed level are coupled by a set of governing equations (e.g. Van Rijn, 1993). A schematic picture of such a model is given in Figure 2.1a (dotted line).

Figure 2-1 Morphological models at present (a) and extensions for sand-mud model (b)

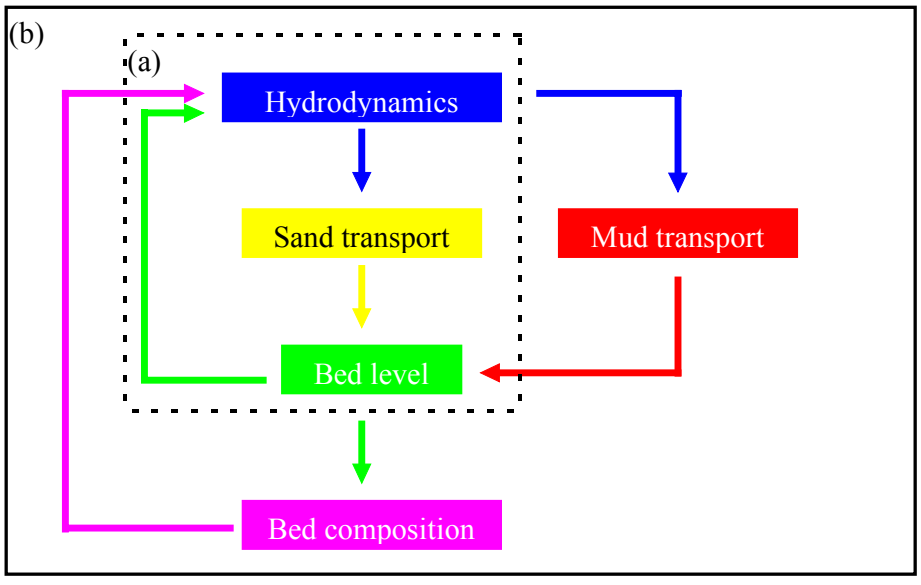

When both non-cohesive and cohesive sediments determine the morphological behaviour significantly, the aforementioned assumptions are no longer valid. Firstly, the bed roughness of non-cohesive and cohesive beds are strongly different (e.g. Van Rijn, 1993). Secondly, non-cohesive and cohesive sediment fractions are both important for bed level changes.

Finally, the bed composition can vary strongly in time and space. Only the first assumption can still be valid if the total sediment concentration in the water column is relatively small.

In this chapter a set of governing equations is proposed for a morphological model with two sediment fractions: a non-cohesive (sand) fraction and a cohesive (mud) fraction. The main extensions to the existing morphological models are:

- two sediment fractions: a sand and a mud fraction;
- bed level changes due to sand and mud exchange;
- non-uniform and time-dependent bed composition;

The extensions to the present morphological models are shown in Figure 2.1b (solid line).

The flow model, the sediment transport model (sand & mud) and the bed model (i.e. bed level and bed composition) are discussed in section 2.2 - 2.4 respectively. Only extensions to the existing sub-models are given. The description is given for three spatial dimensions and one time dimension.

2.2 Flow model

The flow in estuaries is a very complex three-dimensional phenomenon. Often, a distinction is made between currents and (short) waves. Currents are induced by the tide, wind and river discharge. However, density currents due to salinity differences and high sediment concentrations can also be important. The impact of these currents on the bed sediments is twofold. Firstly, currents induce a shear stress at the bed surface, which is an important parameter for the exchange of sediments between the water column and the bed. Secondly, currents transport sediment from one site to another. Short waves are generated by the wind and can significantly intensify the bed shear stress due to currents.

In the morphological model the following initial assumptions with respect to the flow are made. Sediment concentrations in the water column are assumed to be low and interactions between the turbulent water motion and suspended sediment concentration are neglected. Furthermore, short waves are also neglected.

The three-dimensional flow due to currents can be described by a mass balance equation and three momentum equations, but are not given herein (see e.g. Janssen, 1979, Van Rijn, 1993). In these equations the flow variables are the water level (ζ) and three velocity components (u, v, w). These variables are shown in Figure 2-2. The bed level (z_b) and the water depth (H) are also shown.

When the vertical accelerations are small with respect to the gravitational acceleration, the vertical momentum equation can be reduced to the hydrostatic pressure equation. This approximation is called ‘the shallow water assumption’ and is also applied in the morphological model.

Figure 2-2 Flow variables

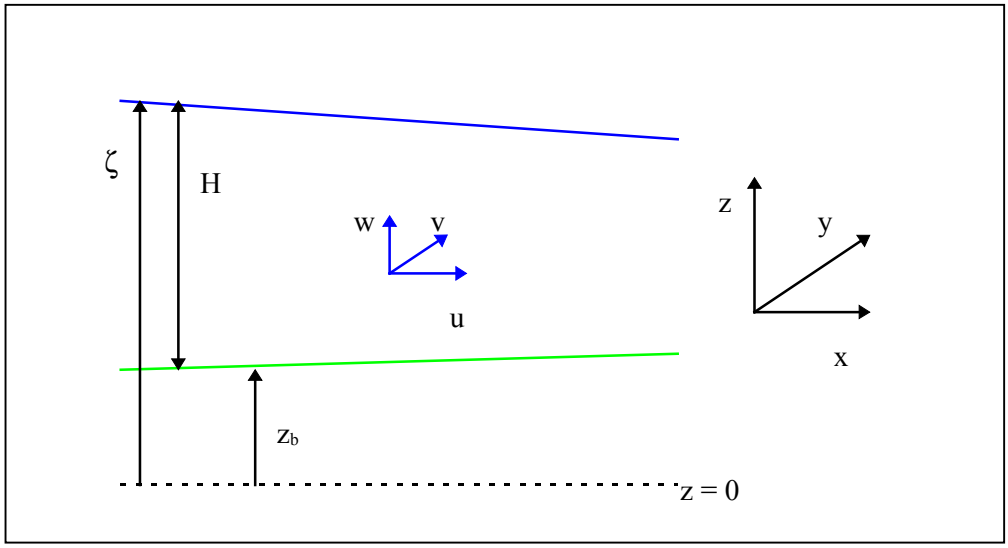

For solving the flow equations, boundary and initial conditions are needed. These conditions do not change due to the introduction of more sediment fractions and are not discussed herein. Besides boundary and initial conditions, two parameters are needed for describing the flow: the fluid mixing coefficients and the roughness coefficient. These are discussed below.

- **Turbulent mixing**

It seems reasonable that for low sediment concentrations the existing turbulent mixing models can be applied. Initially, for horizontal fluid mixing coefficients ($\varepsilon_{f,x}$ and $\varepsilon_{f,y}$) constant values in time and space are used. For the vertical fluid mixing coefficient ($\varepsilon_{f,z}$), the well-known parabolic fluid mixing profile is used:

$$\varepsilon_{f,z} = \frac{z - z_b}{H}\left[1 - \frac{z - z_b}{H}\right]\kappa u_* H \qquad (2.1)$$

in which:

$\varepsilon_{f,z}$ = Vertical fluid mixing coefficient [m^2/s]
z = Vertical co-ordinate [m]
z_b = Bed level [m]
H = Water depth [m]
κ = Von Karman's constant [= 0.4]
u_* = Shear velocity [m/s]

It should be noted that the use of constant fluid mixing coefficients in horizontal directions and a parabolic fluid mixing profile in vertical direction is not essential for the morphological model. More complicated turbulence models (e.g. k-ε model) can be applied as well.

- **Roughness**

An important parameter in the flow equations is the roughness parameter for describing the momentum exchange between the bed and the flow. At present this parameter is often assumed to be constant in time and space due to lack of knowledge. However, it is known that the roughness parameter for non-cohesive sediments strongly depends on the hydraulic conditions and the grain size. Typical values for the Chézy-coefficient in natural open channel flow range from 40 - 60 $m^{1/2}/s$ (Van Rijn, 1993).

For cohesive environments, the Chézy-coefficient is much larger, ranging from 60 - 100 $m^{1/2}/s$ (Van Rijn, 1993). Furthermore, laboratory experiments have shown that bed forms in a sand bed are increasingly suppressed as the mud content is increased. For a certain mud content (i.e. the critical mud content) the bed behaves in a cohesive manner and no bed forms are observed (Torfs, 1995).

The roughness coefficient is very important for the morphological behaviour. Probably, a positive feedback exists between mud deposition and the bed roughness. The feedback mechanism is as follows: when mud deposits at a certain location, the bed roughness decreases. Because the bed roughness decreases, the bed shear stress also decreases and accordingly, mud deposition increases. Consequently, the bed roughness decreases again, and so on.

Although the roughness coefficient strongly depends on the bed composition, it is assumed to be independent of the bed composition initially due to lack of knowledge. It is recommended to analyse the consequences of a varying roughness coefficient in a following phase.

2.3 Sediment transport model

2.3.1 General

Sand and mud are continuously entrained, transported and deposited in estuaries by currents. Due to different sediment properties (e.g. grain size, cohesiveness), the sediment transport characteristics of sand and mud are different.

In general, sand is transported as bed load or suspended load. Bed load occurs at the bed-water interface, suspended load in the water column. A difference between bed load and suspended load transport is that bed load transport instantaneously adapts to the local flow conditions, while suspended load is also determined by upstream conditions. The bed boundary for suspended sand transport is located at a small height (z_a) above the bed level (z_b), the so-called ‘reference’ height. Below this reference height bed load transport occurs. Both bed load and suspended load transport are shown in Figure 2-3.

For low sediment concentrations, mud is only transported in suspension. For high concentrations mud can also be transported in a layer near the bed which is called ‘fluid mud’. In first instance only suspended mud is taken into account (Figure 2-3).

In section 2.3.2 suspended sand and mud transport is discussed. Bed load transport of sand is treated in the section 2.3.3.

Figure 2-3 Sand and mud transport

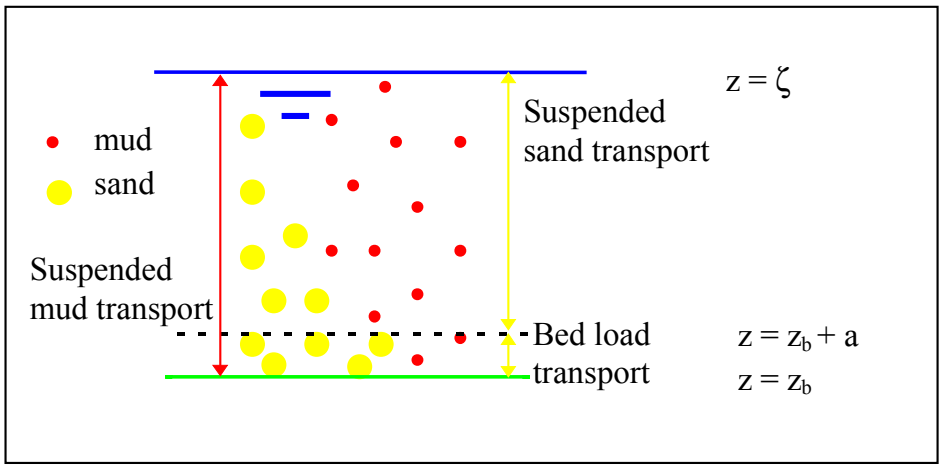

2.3.2 Suspended sediment transport

Sediment in suspension is generally described by an advection-diffusion equation. Deposition experiments have shown that for low sediment concentrations in the water column sand and mud behave independently (Torfs, 1996). Therefore, it seems reasonable that for low sediment concentrations sand and mud in suspension can both be described by an advection-diffusion equation. The equations for sand (2.2) and mud (2.3) are given by:

$$\frac{\partial c_s}{\partial t}+\frac{\partial}{\partial x}\left(uc_s-\varepsilon_x\frac{\partial c_s}{\partial x}\right)+\frac{\partial}{\partial y}\left(vc_s-\varepsilon_y\frac{\partial c_s}{\partial y}\right)=\frac{\partial}{\partial z}\left((w_s-w)c_s+\varepsilon_{s,z}\frac{\partial c_s}{\partial z}\right) \qquad (2.2)$$

$$\frac{\partial c_m}{\partial t}+\frac{\partial}{\partial x}\left(uc_m-\varepsilon_x\frac{\partial c_m}{\partial x}\right)+\frac{\partial}{\partial y}\left(vc_m-\varepsilon_y\frac{\partial c_m}{\partial y}\right)=\frac{\partial}{\partial z}\left((w_m-w)c_m+\varepsilon_{m,z}\frac{\partial c_m}{\partial z}\right) \qquad (2.3)$$

(1) (2a) (2b) (3a) (3b) (4a) (4b)

in which:

c_s = Sand concentration [-]
c_m = Mud concentration [-]
w_s = Settling velocity sand [m/s]
w_m = Settling velocity mud [m/s]
t = Time [s]
x,y,z = Space [m]
u = Flow velocity in x-direction [m/s]
v = Flow velocity in y-direction [m/s]
w = Flow velocity in z-direction [m/s]

ε_x = Sediment mixing coefficient in x-direction [m^2/s]
ε_y = Sediment coefficient in y-direction [m^2/s]
$\varepsilon_{m,z}$ = Sediment mixing coefficient for mud in z-direction [m^2/s]
$\varepsilon_{s,z}$ = Sediment mixing coefficient for sand in z-direction [m^2/s]

In these equations the local change in the sediment concentration at a certain level above the bed is given in term (1) and the (horizontal) sediment fluxes in x and y-directions are given in term (2) and (3) respectively. The right hand side (4) is the sediment flux in vertical direction. The first part of these fluxes is due to advection (2a, 3a & 4a) and the second part due to diffusion (2b, 3b & 4b).

In solving the advection-diffusion equations for sand and mud (2.2 and 2.3), settling velocities (w_s and w_m) and sediment mixing coefficients in both horizontal (ε_x and ε_y) and vertical ($\varepsilon_{m,z}$ and $\varepsilon_{s,z}$) directions must be prescribed. These coefficients are discussed below:

- **Settling velocity for sand and mud**

The setting velocity for sand (w_s) is directly related to the sand grain size and assumed to be constant in time and space. Due to the ability of forming flocs, the settling velocity for mud (w_m) is generally not constant in time and space but strongly depends on turbulent intensity and the mud concentration in the water column (Winterwerp, 1999). Initially the settling velocity of mud is assumed to be constant in time and space. It is recommended to include and analyse the effect of a time- and space-dependent settling velocity for mud in a following phase.

- **Turbulent mixing**

Horizontal turbulent mixing is often negligible compared to horizontal advection of sediment. Herein, the horizontal sediment mixing coefficients (ε_x and ε_y) are assumed to be constant in time and space and equal to the horizontal fluid mixing coefficients (see section 2.2).

The vertical sediment mixing coefficient is assumed to be proportional to the vertical fluid mixing coefficient ($\varepsilon_{f,z}$) (see section 2.2):

$$\varepsilon_{i,z} = \beta_i \varepsilon_{f,z} \tag{2.4}$$

in which:
$\varepsilon_{i,z}$ = Sediment mixing coefficient of fraction i at height z above the bed [m^2/s]
β_i = Efficiency factor for turbulent sediment transport [-]

For the mud fraction the proposed value by Lesser (2000) $\beta_m = 1.4$ is applied. This value is generally used for conservative constituents and very fine particles.

For sand, Van Rijn's expression is used (Van Rijn, 1993):

$$\beta_s = 1 + 2\left[\frac{w_s}{u_*}\right]^2 \tag{2.5}$$

The value β_s is limited to the range $1 < \beta_s < 1.5$.

Furthermore, appropriate initial and boundary conditions are needed for solving the advection-diffusion equations for sand and mud. These conditions are discussed below. It should be noted that only the bed boundary condition is drastically changed due to the introduction of more sediment fractions compared with the existing one-fraction models.

- **Initial conditions**

At time t = 0 the sand concentration c_s (t = 0, x, y, z) and the mud concentration c_m (t = 0, x, y, z) has to be specified. For sand the initial concentration is set to zero and for mud, the initial concentration is set to the upstream boundary concentration. This condition is usually not very important because the influence will disappear after some time.

- **Inflow boundary conditions**

At inflow boundaries, sand and mud concentrations have to be given. For sand, a equilibrium sand concentration profile is used: the so-called Rouse profile. For mud an equilibrium mud concentration does not exist for low sediment concentrations. Therefore, a specific value is prescribed at the inflow boundary. Furthermore, the mud concentration is assumed to be uniform in vertical direction at this boundary.

- **Outflow, closed and water surface boundary conditions**

At these boundaries the conditions, as described by the existing one fraction models, are adequate. For the outflow boundaries, a ‘weak’ condition is often applied. This means that the first or second derivative of the concentration normal to the boundary is set to zero. For closed and water surface boundaries, the sediment fluxes across the boundary are assumed to be zero.

- **Bed boundary condition**

The only boundary condition which changes drastically due to presence of sand and mud in the bed is the boundary condition at the bed-water interface. The bed boundary for suspended sand transport is located at a small height (z_a) above the bed level (z_b), the so-called ‘reference’ height (Figure 2-3). Below this level the sand concentration is assumed to adapt instantaneously to the local flow conditions and is always equal to the equilibrium sand concentration. For low mud concentrations in the water column, mud is only transported in suspension and it seems reasonable to assume the bed boundary for suspended mud at the bed level ($z = z_b$).

For sand two bed boundary conditions are often used: a concentration type and a gradient type (Wang, 1989). The concentration type assumes that the sediment concentration at the bed boundary adapts instantaneously to the equilibrium value. The gradient type describes the upward sediment flux at the bed boundary. For suspended mud transport the net flux is always described at the bed boundary (e.g. Partheniades - Krone formula). The net flux can also be given for suspended sand and is used herein for the bed boundary condition.

The net flux at the bed boundary for sand (2.6) and mud (2.7) can be expressed as:

$$\left[w_s c_s + \varepsilon_{z,s} \frac{\partial c_s}{\partial z} \right]_{z=z_a+z_b} = F_s \tag{2.6}$$

$$\left[w_m c_m + \varepsilon_{z,m} \frac{\partial c_m}{\partial z} \right]_{z=z_b} = F_m \tag{2.7}$$

in which:
F_s = Net upward suspended sand flux at height $z = z_a$ [m/s]
F_m = Net upward suspended mud flux at height $z = z_b$ [m/s]

Figure 2-4 Net suspended sand and mud flux at bed boundary

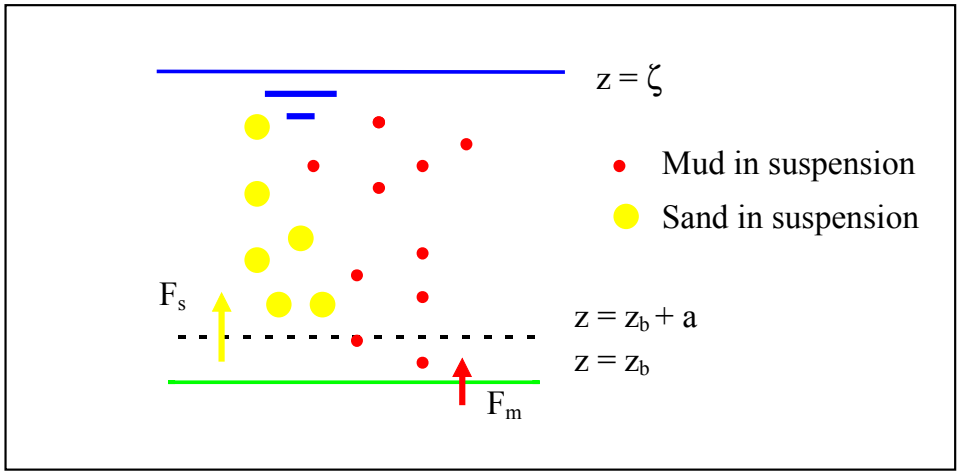

Both F_s and F_m are shown in Figure 2-4. It should be noted that positive F_s and F_m are net upward fluxes from the bed to the water column, which are the result of both downward (deposition) and upward (erosion) fluxes. The used expressions for F_s and F_m are discussed below.

Deposition experiments showed that sand and mud do not interact in the water column in case of low sediment concentrations (Torfs, 1996). It seems reasonable that under these conditions the classical deposition fluxes for sand and mud are valid. For mud, Krone's deposition formula is applied and for sand, the downward flux is given by the actual sand concentration near the bed and the settling velocity.

The upward sediment flux from the bed into the water column strongly depends on the bed composition at the bed surface. From laboratory experiments it was concluded that two regimes can be distinguished: a non-cohesive and a cohesive regime (Van Ledden & Wang, 2000). The clay content (% < 2 μm) is the governing parameter for the transition between both regimes. When the clay content is less than 5 - 10%, the bed behaves more or less non-cohesive. Sand is transported as bed load or suspended load, depending on the hydrodynamic conditions. Mud is easily washed out from the top layer. For a clay content

higher than 5 - 10%, the bed behaves cohesively. Sand and mud do not act independently in the bed, but are eroded at the same time.

The importance of the clay content (% < 2 μm) for the erosion process also suggests that the permeability of the bed is an important erosion parameter for a sand-mud bed. In Figure 2-5 the permeability C_v is shown as function of the sand, silt and clay content. The more or less horizontal lines with the same permeability show that this parameter mainly depends on the clay content. Furthermore, the permeability strongly decreases with increasing clay content. It is recommended to pay special attention to the role of the bed permeability during erosion experiments with sand-mud mixtures.

Figure 2-5 Sand-silt-clay triangle and permeability C_v

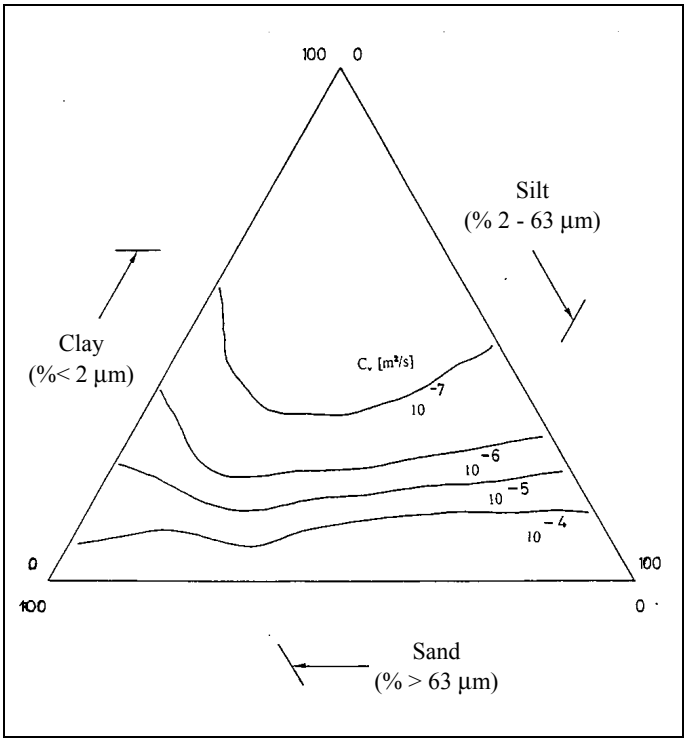

Field data suggest a strong correlation between the clay (% < 2 μm) and the silt content (% 2 - 63 μm) in the bed for tidal systems (Van Ledden, 2000). This indicates that a critical mud content (% < 63 μm) can also be used for the transition between non-cohesive and cohesive behaviour. It should be noted that the critical mud content is a site specific value. The critical mud content is denoted as p_{cr} and the mud content in the bed is denoted as p_m.

When the mud content in the bed (p_m) is less than the critical mud content (p_{cr}), sand and mud are assumed to behave independently during erosion. The classical sand transport formulas are more or less valid (Torfs, 1995). For the erosion of mud the Partheniades formula is assumed to be valid. Because the mud content can vary, the mud content in the bed (p_m) is added to the traditional formula. Combining the downward and the upward flux, the net sediment fluxes at the bed-water interface for sand (F_s) and mud (F_m) in suspension are prescribed as follows for $p_m < p_{m,cr}$:

$$F_s = w_s\left(c_a - c_s\right)$$
$$F_m = p_m M\left[\frac{\tau_b}{\tau_{e,nc}} - 1\right]H\left[\frac{\tau_b}{\tau_{e,nc}} - 1\right] - w_m c_m\left[1 - \frac{\tau_b}{\tau_d}\right]H\left[1 - \frac{\tau_b}{\tau_d}\right] \tag{2.8}$$

in which:
c_a = Equilibrium sand concentration at height $z = z_a$ [-]
c_s = Sand concentration at height $z = z_a$ [-]
c_m = Mud concentration at $z = z_b$ [-]
H = Step function [-]
M = Erosion parameter [m/s]
p_m = Mud content at bed-water interface [-]
$\tau_{e,nc}$ = Critical erosion shear stress for non-cohesive regime [N/m^2]
τ_b = Bed shear stress [N/m^2]
τ_d = Critical deposition shear stress [N/m^2]

Various expressions are used for the equilibrium sand concentration near the bed (c_a). Herein, the expression of Van Rijn is used (Van Rijn, 1993). The equilibrium concentration near the bed (c_a) is given by:

$$c_a = 0.015\frac{d_{50}}{a}\frac{T^{1.5}}{D_*^{0.3}} \tag{2.9}$$

in which:
d_{50} = Average grain size [m]
a = Reference height [m]
T = Transport parameter [-]
D_* = Dimensionless diameter [-]

When the mud content in the bed (p_m) is higher than the critical mud content (p_{cr}) sand and mud are assumed to erode at the same time and with the same rate. The Partheniades formula seems to be the most obvious formula for describing the upward flux of mud and sand. The formula is adapted by introducing a parameter for the sand and mud content in the bed. The deposition fluxes do not differ from the deposition fluxes given in (2.8). For $p_m > p_{m,cr}$ the net sediment flux for sand (F_s) and mud (F_m) are respectively given by:

$$F_s = \left(1 - p_m\right)M\left[\frac{\tau_b}{\tau_{e,c}} - 1\right]H\left[\frac{\tau_b}{\tau_{e,c}} - 1\right] - w_s c_s$$
$$F_m = p_m M\left[\frac{\tau_b}{\tau_{e,c}} - 1\right]H\left[\frac{\tau_b}{\tau_{e,c}} - 1\right] - w_m c_m\left[1 - \frac{\tau_b}{\tau_d}\right]H\left[1 - \frac{\tau_b}{\tau_d}\right] \tag{2.10}$$

in which:
$\tau_{e,c}$ = Critical erosion shear stress for cohesive regime [N/m^2]

It should be noted that the experimental evidence for the erosion flux in particular is rather weak. It is recommended to carry out more laboratory experiments with mixed sand-mud beds in order to derive more reliable expressions for the erosion fluxes of sand and mud.

2.3.3 Bed load transport

Laboratory experiments have shown that ripples and dunes are increasingly suppressed with increasing mud content in a sand bed. Above a certain critical mud content, no ripples were observed and the bed behaves cohesively (Torfs, 1995).

It is assumed that when the bed contains no mud classical bed load transport formulas can be applied. This bed load transport rate is denoted as $S_{b,0}$. As a simple approach the bed load transport rate is assumed to decrease linearly in the non-cohesive regime. For the cohesive regime, the bed load transport rate is assumed to be zero.

The bed load transport rate can be given as follows:

$$\begin{aligned} S_b &= \left(1 - \frac{p_m}{p_{cr}}\right) S_{b,0} \qquad p_m < p_{cr} \\ S_b &= 0 \qquad\qquad\qquad\quad p_m > p_{cr} \end{aligned} \tag{2.11}$$

in which:
S_b = Bed load transport rate [m^2/s]
$S_{b,0}$ = Bed load transport rate for sand only [m^2/s]
p_m = Mud content at the bed water interface [-]
p_{cr} = Critical mud content [-]

For the bed load transport rate for sand only ($S_{b,0}$) the transport formula of Van Rijn is applied. This formula is given by:

$$S_{b,0} = 0.5 u_* d_{50} D_*^{-0.3} T \tag{2.12}$$

in which:
$S_{b,0}$ = Bed load transport rate for sand only [m^2/s]

It should be noted that the experimental evidence for the bed load transport rate in case of a mixed sand-mud bed is rather weak. It is recommended to carry out laboratory experiments with sand-mud beds in order to derive a more reliable expression for the bed load transport rate of sand.

2.4 Bed model

2.4.1 Bed level

When the bed contains sand as well as mud, bed level changes are caused by erosion and/or deposition of both sediment fractions and bed density variations. In first instance, the bed density is assumed to be constant in time and space. This implicates that consolidation effects and filling of pores between sand particles by fine mud flocs/particles are both neglected.

By assuming a constant bed density in time and space, the bed level change is given by:

$$(1-\varepsilon_p)\frac{\partial z_b}{\partial t} = -F_m - F_s - \frac{\partial S_b}{\partial x} - \frac{\partial S_b}{\partial y} \tag{2.13}$$

in which:
z_b = Bed level [m]
ε_p = Bed porosity [-]

In (2.13) the left hand side expresses the bed level change. At the right hand side the net vertical exchanges due to suspended mud transport (F_m), suspended sand transport (F_s) and horizontal gradients in the bed load transport rate ($\partial S_b/\partial x$ and $\partial S_b/\partial y$) are given respectively.

- **Boundary condition**

For the bed level a boundary condition is only needed at inflow boundaries. Herein, the bed level is assumed to remain unchanged at inflow boundaries.

- **Initial condition**

At time t = 0 the bed level z_b (t = 0, x, y) has to be specified.

2.4.2 Bed composition

There are two possible reasons for changes in the bed composition. Firstly, at the bed-water interface the composition can change due to changes in the upward and downward fluxes of sand and mud. Secondly, the composition in the bed can also change due to mixing of sediment particles. Mixing is often divided into two contributions. The first mixing type is caused by small-scale disturbances at the bed-water interface (e.g. ripples). It seems reasonable that the mixing intensity due to these disturbances decreases with increasing distance from the bed surface.

The second mixing type is caused by biological activity (e.g. bioturbation by organisms). This is often called ‘local biological mixing’ because the sediment flux depends on the local composition gradients and the net flux of a certain sediment fraction is always directed from areas with a higher to areas with a lower content of that fraction (Boudreau, 1997).

Organisms can also cause 'non-local' mixing when they transport a specific sediment size (e.g. mud) from one site to another. The flux does not depend on the composition gradients and transport can even take place from a site with a low mud content to a high mud content (Boudreau, 1997). In the first instance only mixing due to small-scale disturbances and local biological mixing are taken into account.

For modelling the bed composition, a distinction is often made between the active layer and the sub layer. In the active layer the mud content (p_m) varies in time and space due to the aforementioned contributions of erosion and/or deposition at the bed level and mixing within the bed. In the sub layer the mud content ($p_{m,sub}$) is assumed to remain unchanged. Both layers and the mud content are sketched in Figure 2-6.

Figure 2-6 Definitions bed composition

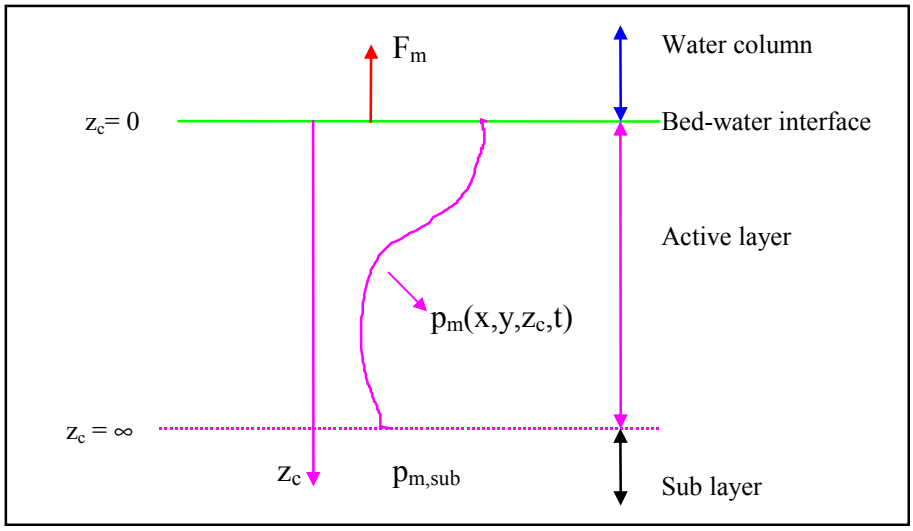

In a Lagrangian co-ordinate system the mud content can be described with an advection-diffusion equation (Armanini, 1995). The advection-diffusion equation is equal to:

$$\frac{\partial p_m}{\partial t} + \frac{\partial z_b}{\partial t}\frac{\partial p_m}{\partial z_c} - \frac{\partial}{\partial z_c}\left(\Xi_{mix}\frac{\partial p_m}{\partial z_c}\right) = 0 \qquad (2.14)$$

(1) (2) (3)

in which:
z_c = Distance from the bed level [m]
p_m = Mud content at distance z_c below bed level [-]
Ξ_{mix}= Mixing coefficient at distance z_c below bed level [m^2/s]

It should be noted that the vertical co-ordinate z_c is positive in downward direction (Figure 2-6) and the origin is always at the bed-water interface. In the above mentioned advection-diffusion equation (2.14) the local change in mud content at a certain height z_c below the

bed level is given by term (1). The local mud content varies due to bed level changes (term 2) and physical and /or biological mixing in the bed (term 3).

In case of two sediment fractions (i.e. sand and mud), the changes in the sand content in the bed can be easily given as follows:

$$p_s = 1 - p_m \tag{2.15}$$

in which:
p_s = Sand content at depth z below bed level [-]

The advection-diffusion equation can only be solved with appropriate initial conditions, boundary conditions and a mixing coefficient. These items are discussed below.

- **Initial conditions**

At time t = 0 the mud content p_m (t = 0, x, y, z_c) has to be specified.

- **Boundary conditions**

For solving the given advection-diffusion equation two boundary conditions are needed: at the bed-water interface and far below the bed surface. In case of two sediment fractions, boundary conditions are only needed for one sediment fraction because the other fraction is easily solved by applying (2.15). Herein, boundary conditions are only given for the mud fraction.

At the bed-water interface ($z_c = 0$) the supended mud flux (F_m) is prescribed (Figure 2-6). This flux is already discussed in the section 2.3.2. The boundary condition at the bed surface ($z_c = 0$) for the mud content in the bed (p_m) is equal to:

$$\left[\frac{\partial z_b}{\partial t} p_m + \Xi_{mix} \frac{\partial p_m}{\partial z_c} \right]_{z_c=0} = F_m \tag{2.16}$$

in which:
F_m = Net mud flux at bed surface [m/s]

Far below the bed level ($z_c = \infty$) the bed boundary condition depends on the direction of the bed level change ($\partial z_b/\partial t$). In case of deposition ($\partial z_b/\partial t > 0$), this boundary is an 'outflow' boundary, because a Langragian approach is applied. At an outflow boundary a 'weak' boundary condition is sufficient and it seems reasonable to assume that the diffusive flux equals zero far below the boundary. In case of erosion ($\partial z_b/\partial t < 0$), the mud content at the boundary must be prescribed and is equal to the mud content of the sub layer (Figure 2-6). Both boundary conditions are given by:

$$\begin{aligned} &\left[\frac{\partial p_m}{\partial z_c} \right]_{z_c=\infty} = 0 \qquad && \frac{\partial z_b}{\partial t} > 0 \\ &\left[p_m \right]_{z_c=\infty} = p_{m,sub} \qquad && \frac{\partial z_b}{\partial t} < 0 \end{aligned} \tag{2.17}$$

in which:
$p_{m,sub}$ = Mud content in the sub layer [-]

- **Mixing coefficient**

As already discussed, mixing can occur due to small-scale disturbances at the bed-water interface and due to organisms. The first type is called 'physical mixing' and the second type 'biological mixing'. For both types a mixing coefficient must be prescribed.

It seems reasonable that the physical mixing coefficient increases with increasing current velocity near the bed surface and decreases exponentially with increasing distance from the bed. Armanini (1995) proposed the following function for the physical mixing coefficient ($\Xi_{mix,p}$):

$$\Xi_{mix,p} = \alpha_{mix,p} u_* d_{50} e^{-\frac{z_c}{L_{mix,p}}} \tag{2.18}$$

in which:
$\Xi_{mix,p}$ = Mixing due to small-scale physical disturbances within the bed [m^2/s]
$\alpha_{mix,p}$ = Empirical coefficient [-]
$L_{mix,p}$ = Mixing length due to for small-scale physical disturbances [m]

The physical mixing coefficient ($\Xi_{mix,p}$) is shown in Figure 2-7 (solid line).

Figure 2-7 Physical and biological mixing coefficient

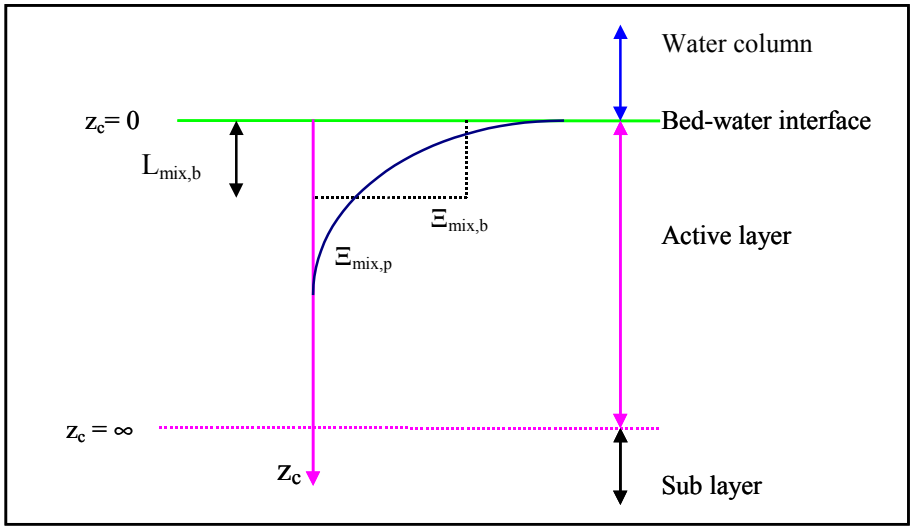

In general, biological mixing occurs only in the upper layer near the bed surface (e.g. upper ten centimetres), the so-called 'biological activity zone'. For biological mixing it seems reasonable to assume a constant mixing coefficient over a certain distance below the bed surface (L_b) and no mixing below the biological activity zone. The biological mixing parameter ($\Xi_{mix,b}$) can then be described as follows:

$$\Xi_{mix,b} = \Xi_{mix,b} H\left[1 - \frac{z_c}{L_{mix,b}}\right] \tag{2.19}$$

in which:
$\Xi_{mix,b}$ = Mixing due to biological activity [m^2/s]
$L_{mix,b}$ = Biological activity zone [m]

The biological mixing coefficient ($\Xi_{mix,b}$) and the biological activity zone (L_b) are shown in Figure 2-7 (dotted line).

The total mixing is the sum of both physical and biological mixing and is thus written as follows:

$$\Xi_{mix} = \Xi_{mix,b} H\left[1 - \frac{z_c}{L_{mix,b}}\right] + \alpha_{mix,p} u_* d_{50} e^{-\frac{z_c}{L_{mix,p}}} \tag{2.20}$$

in which:
Ξ_{mix}= Total mixing at distance z_c below the bed surface [m^2/s]

3 Numerical modelling

3.1 Introduction

In the previous chapter, the governing equations are discussed for a process-based morphological model with two sediment fractions: sand and mud. Only for very schematised situations and by neglecting various terms within these equations an analytical analysis can be made (Van Ledden & Wang, 2000). For more complicated situations the governing equations must be solved by a numerical model.

In this chapter the implementation of the governing equations in a numerical model is discussed. The starting point for the numerical implementation is DELFT3D-FLOW, a software package which is developed at WL | DELFT HYDRAULICS. In DELFT3D-FLOW the hydrodynamics (waves and currents), sediment transport (suspended and bed load) and bed level changes for non-cohesive sediments can be computed. An overview of the existing model is given by Lesser (2000). Herein, only modifications in DELFT3D-FLOW are discussed (section 3.2). Next, some numerical aspects are discussed (section 3.3).

3.2 Modifications in DELFT3D-FLOW

3.2.1 Overview

Before discussing the modifications in DELFT3D-FLOW a short overview is given of the three-dimensional numerical computation (Figure 3.1). The model area is discretisized in computational cells (index nm) in horizontal direction. The water column (index k) and the bed (index j) of each computational cell is discretisized in vertical direction. The layer thickness in the water column is not fixed, but is a constant percentage of the water depth. The layer thickness in the bed is fixed.

- **Flow computation**

The flow is computed by solving the shallow water equations (see section 2.2) with appropriate boundary and initial conditions. The computed variables are the water level (ζ) and current velocities in three directions (u, v, w) in each cell with index (nm, k). No adaptations are made with respect to the flow equations herein.

- **Sediment transport computation**

Thereafter, the suspended sediment concentrations are computed for each cell with index (nm,k) by solving the advection-diffusion equation for two sediment fractions: sand (subscript s) and mud (subscript m) with appropriate initial and boundary conditions (see section 2.3.2). The computed variables are the sand concentration (c_s) and the mud concentration (c_m) for each cell with index (nm, k). Because the boundary condition at the

bed-water interface depends on the mud content in the bed, the computation of the boundary condition at the bed-water interface is adapted herein.
Furthermore, the bed load transport rate is computed (S_b) for each cell with index (nm). Because the bed load transport rate depends on the mud content in the bed, the computation of the bed load transport rate is also adapted.

Figure 3-1 Overview of discretisation

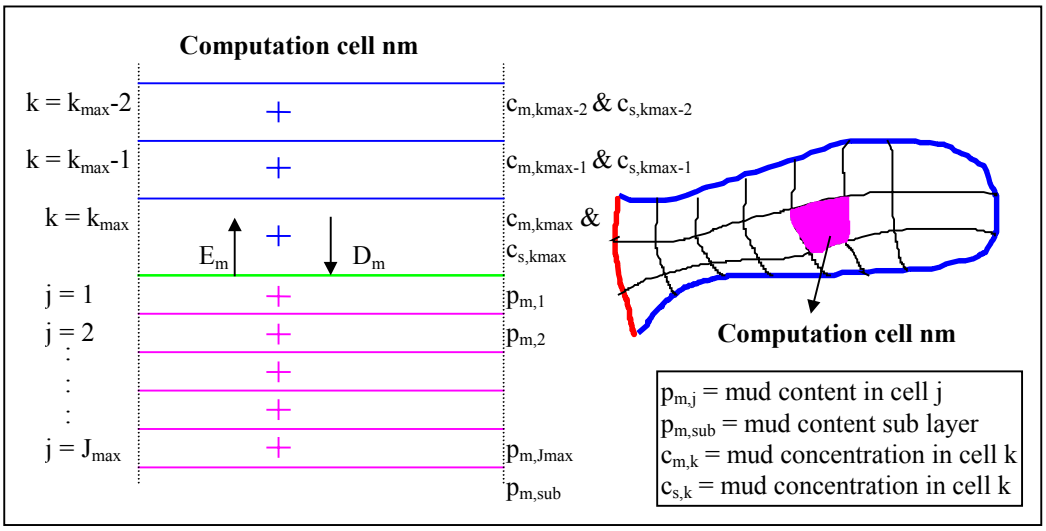

- **Bed level**

Based on the bed load transport gradients and the exchange of suspended sediment, the bed level changes are calculated in each cell with index (nm) by solving the bed level equation (see section 2.4.1). The computed variable is the bed level (z_b). Because the bed level depends on both sand and mud exchange, the bed level computation is adapted.

- **Bed composition**

Finally, the bed composition changes are calculated by solving an advection-diffusion equation (see section 2.4.2) for each cell with index (nm, j). The total number of cells in the bed is denoted by J_{max}. A new routine is constructed for adding the bed composition computation to the present model.

The modifications for suspended and bed load transport, the bed level and the bed composition computation are discussed in section 3.2.2 - 3.2.4 respectively.

Various new input parameters are needed for the morphological computation with a sand and a mud fraction. A new input file **[BEDCOM.inp]** is constructed for all parameter values needed for the bed composition computation. The default value, the variable name, the description and the unit of these parameters are summarized in Table 3-1.

It should be noted that these parameters are all constant during the whole computation. Moreover, the critical mud content (% < 63 µm) **[PMUDCR]** is a site-specific value and depends on the ratio between the silt content (% 2 - 63 µm) and the clay content (% < 2 µm) (see also 2.3.2).

Table 3-1 Parameters in inputfile BEDCOM.inp

Value	Variable	Description	Unit
0.30	PMUDCR	Critical mud content (% < 63 μm) for transition between non-cohesive and cohesive behaviour	[-]
0.50	TAUENC	Critical erosion shear stress for non-cohesive behaviour	[N/m^2]
0.50	TAUEC	Critical erosion shear stress for cohesive behaviour	[N/m^2]
10^{-7}	M	Erosion rate	[m/s]
0.25	TAUD	Critical deposition shear stress for mud	[N/m^2]
0.0005	WSM	Settling velocity for mud	[m/s]
10^{-8}	EB	Biological mixing coefficient	[m^2/s]
0.10	LB	Biological mixing length	[m]
0.0005	ALFA	Physical mixing coefficient	[-]
0.25	LP	Physical mixing length	[m]
40	JMAX	Number of layers for bed composition computation	[-]
0.10	DELTAZ	Thickness of layer for bed composition computation	[m]
0.00	PMUD0	Mud content at time t = 0	[-]
0.40	BEDPOR	Bed porosity	[-]
0.00	MUDSUB	Mud content sub layer	[-]

3.2.2 Sediment transport

- **Suspended sediment transport**

At present DELFT3D-FLOW has already the possibility to solve the advection-diffusion equation for more than one sediment fraction (Lesser, 2000). The only adaptation to be made for suspended sediment transport is adding the process description for sand and mud exchange at the bed boundary. The changes are being carried out in routine **[EROSED.f]**.

In this routine the exchange of suspended sediment is calculated at a certain time step for each horizontal cell (nm) (Figure 3-1). For a combined sand-mud model only the upward fluxes of sand and mud depend on the actual mud content at the bed surface (section 2.3.2). When the mud content in the first layer (index j = 1) of the bed ($p_{m,1}$) is larger than the critical mud content (p_{cr}), then the erosion fluxes for both sand (E_s) and mud (E_m) are calculated as follows:

$$E_m = p_{m,1} M \left[\frac{\tau_b}{\tau_{e,c}} - 1 \right]$$
$$E_s = \left(1 - p_{m,1}\right) M \left[\frac{\tau_b}{\tau_{e,c}} - 1 \right] \tag{3.1}$$

in which:
E_m = Erosion rate of mud [m/s]
E_s = Erosion rate of sand [m/s]
τ_b = Bed shear stress at time t [N/m^2]
$\tau_{e,c}$ = Critical bed shear stress for erosion in cohesive regime [N/m^2]
$p_{m,1}$ = Mud content in the first cell of the bed (j = 1) at time t [-]
M = Erosion rate [m/s]

When the mud content in the first layer of the bed ($p_{m,1}$) is lower than the critical mud content (p_{cr}), the erosion flux for mud (E_m) is calculated as follows:

$$E_m = p_{m,1} M \left[\frac{\tau_b}{\tau_{e,nc}} - 1 \right] \tag{3.2}$$

in which:
$\tau_{e,nc}$ = Critical bed shear stress for erosion in non-cohesive regime [N/m^2]

The erosion flux for sand is equal to the classical erosion flux and is not modified in DELFT3D-FLOW. Furthermore, the downward flux for sand is not modified since this flux does not depend on the actual mud content in the bed. The numerical computation of classical suspended sand exchange is extensively discussed by Lesser (2000) and are not repeated here.

The downward flux for mud is calculated as follows:

$$D_m = w_m c_m \left[1 - \frac{\tau_b}{\tau_d} \right] \tag{3.3}$$

in which:
τ_d = Critical bed shear stress for mud deposition [N/m^2]
D_m = Deposition rate of mud [m/s]
c_m = Mud concentration at time t = t + dt and in cell k = k_{max} [-]

It should be noted that the deposition fluxes for both sand and mud are calculated implicitly. Therefore, the mud concentration (c_m) in the expression for the downward flux (3.3) is at the time step (t + dt).

After calculation of the upward erosion fluxes it is checked if there is enough sediment available in the first layer of the bed. If the amount of mud and/or sand is too low, the upward fluxes for sand and mud are equal to the available amount of sand and mud in the first layer of the bed respectively.

- **Bed load transport**

The bed load transport rate for each cell (index nm) at a certain time step is also calculated in the routine **[EROSED.f]**. When the mud content in the first layer ($p_{m,1}$) is higher than the critical mud content (p_{cr}), the bed load transport rate is set to zero. When the actual mud content is lower than the critical mud content, the bed load transport rate is equal to:

$$S_b = \left(1 - p_{m,1}\right) S_{b,0} \tag{3.4}$$

in which:
$S_{b,0}$ = Bed load transport rate of sand without mud [m^2/s]

3.2.3 Bed level

The computation of the bed level equation is carried out in **[BOTTOM.F]** and is not adapted herein. The discretisized bed level equation is given by:

$$\frac{z^{n+1} - z^n}{N\Delta t} = \frac{\rho_s}{\rho_b}\left(-\frac{S_b^n - S_{bux}^n}{\Delta x} - \frac{S_b^n - S_{buy}^n}{\Delta y} + D_m^n + D_s^n - E_m^n - E_s^n \right) \tag{3.5}$$

in which:
z = Bed level [m]
Δt = Time step [s]
N = Morphological factor [-]
n = Time index including morphological factor [-]
S_{bux} = Bed load transport rate in upstream cell in x-direction [m^2/s]
S_{buy} = Bed load transport rate in upstream cell in y-direction [m^2/s]
Δx = Spatial step in x-direction [m]
Δy = Spatial step in y-direction [m]
ρ_s = Sediment density [kg/m^3]
ρ_b = Bed density [kg/m^3]
D_m = Deposition flux of mud [m/s]
E_m = Erosion flux of mud [m/s]
D_s = Deposition flux of suspended sand [m/s]
E_s = Erosion flux of suspended sand [m/s]

It should be noted that a morphological factor (N) appears in the given equation for the bed level, because for small Froude numbers the time scale for morphological changes is generally much larger than for changes in the flow. To reduce the computation time, a morphological factor (N) is introduced, whereby the morphological changes are scaled up with the morphological factor N. The morphological factor N expresses the ratio between the time step for the bed level ($N\Delta t$) (and bed composition, see section 3.2.4) and the time step for the flow and suspended sediment transport (Δt). When a morphological factor is applied, the morphological changes can have a significant impact on the flow in one time step.

3.2.4 Bed composition

The main modification to the present DELFT3D-FLOW model is the computation of the bed composition in various layers. A new routine is created **[MUDC.F]** in which the advection-diffusion equation for the bed composition is solved for each cell nm (Figure 3-1).

The advection-diffusion equation is discretisized by using an FTCS-scheme (e.g. Vreugdenhil, 1989). This numerical scheme is central in space and forward in time. The discretisized equation for the mud content in the bed is given by:

$$\begin{aligned}
&\frac{p_{m,j}^{n+1}-p_{m,j}^{n}}{N\Delta t}=-\frac{s_{m,j+1/2}^{n}-s_{m,j-1/2}^{n}}{\Delta z}\\
&s_{m,j+1/2}^{n}=\frac{1}{2}u_z^n\left(p_{m,j+1}^{n}+p_{m,j}^{n}\right)-\Xi_{j+1/2}^{n}\frac{p_{m,j+1}^{n}-p_{m,j}^{n}}{\Delta z}\\
&s_{m,j-1/2}^{n}=\frac{1}{2}u_z^n\left(p_{m,j}^{n}+p_{m,j-1}^{n}\right)-\Xi_{j-1/2}^{n}\frac{p_{m,j}^{n}-p_{m,j-1}^{n}}{\Delta z}
\end{aligned} \tag{3.6}$$

in which:
p_m = Mud content at level z below bed surface [-]
s = Sediment flux in the bed [m^2/s]
u = Bed level velocity [m/s]
Ξ = Mixing coefficient [m^2/s]
Δz = Spatial step in the bed [m]
Δt = Time step [s]
N = Morphological factor [-]
n = Index for time step [-]
j = Cell number in the bed [-]

Rewriting of the above given equation gives an expression for the mud content at time step t = t + dt as a function of the mud content at time step t = t:

$$\begin{aligned}
&p_{m,j}^{n+1}=p_{m,j}^{n}+N\Delta t\left[a_{j+1}^{n}p_{m,j+1}^{n}+a_j^{n}p_{m,j}^{n}+a_{j-1}^{n}p_{m,j-1}^{n}\right]\\
&a_{j+1}^{n}=-\frac{u_z^n}{2\Delta z}+\frac{\Xi_{j+1/2}^{n}}{\Delta z^2}\\
&a_j^{n}=-\frac{\Xi_{j-1/2}^{n}}{\Delta z^2}-\frac{\Xi_{j+1/2}^{n}}{\Delta z^2}\\
&a_{j-1}^{n}=+\frac{u_z^n}{2\Delta z}+\frac{\Xi_{j-1/2}^{n}}{\Delta z^2}
\end{aligned} \tag{3.7}$$

in which:
a_j = Numerical coefficient for cell j [-]

At the boundaries the boundary conditions must be used. At the bed water interface (j = 1) the discretised equation for the mud content reads:

$$\frac{p_{m,1}^{n+1} - p_{m,1}^{n}}{N\Delta t} = -\frac{s_{m,1+1/2}^{n} - F_m^n}{\Delta z}$$
$$s_{m,1+1/2}^{n} = \frac{1}{2}u_z^n\left(p_{m,2}^{n} + p_{m,1}^{n}\right) - \Xi_{1+1/2}^{n}\frac{p_{m,2}^{n} - p_{m,1}^{n}}{\Delta z} \qquad (3.8)$$
$$F_m^n = \frac{\rho_s}{\rho_b}\left[D_m^n - E_m^n\right]$$

in which:
F_m = Mud exchange between bed and water column [-]

Rewriting of the above given equation gives an explicit expression for the mud content in the first cell (j = 1) at time step t = t + dt:

$$p_{m,1}^{n+1} = p_{m,1}^{n} + N\Delta t\left[\frac{1}{\Delta z}\frac{\rho_s}{\rho_b}\left[D_m^n - E_m^n\right] + a_1^n p_{m,1}^{n} + a_2^n p_{m,2}^{n}\right]$$
$$a_1^n = -\frac{1}{2\Delta z}u_z^n + \frac{\Xi_{1+1/2}^{n}}{\Delta z} \qquad (3.9)$$
$$a_2^n = -\frac{1}{2\Delta z}u_z^n - \frac{\Xi_{1+1/2}^{n}}{\Delta z}$$

For cell j = J_{max} the discretised equation is almost equal to the discretisized equation for the inner cells, but diffusion at the boundary (j = J_{max} +1/2) is neglected.

$$p_{m,J_{max}}^{n+1} = p_{m,J_{max}}^{n} + N\Delta t\left[a_{J_{max}+1}^{n} p_{m,J_{max}+1}^{n} + a_{J_{max}}^{n} p_{i,J_{max}}^{n} + a_{J_{max}-1}^{n} p_{m,J_{max}-1}^{n}\right]$$
$$a_{J_{max}+1}^{n} = -\frac{u_z^n}{2\Delta z}$$
$$a_{J_{max}}^{n} = -\frac{\Xi_{j-1/2}^{n}}{\Delta z^2} \qquad (3.10)$$
$$a_{J_{max}-1}^{n} = +\frac{u_z^n}{2\Delta z} + \frac{\Xi_{j-1/2}^{n}}{\Delta z^2}$$

For the non-existing cell j = J_{max+1} the sub layer is introduced. Depending on the bed velocity direction, the content of the sub layer is adapted. When the bed level velocity is positive (net deposition), the content of the sub layer is equal to the content of the lowest cell j = J_{max}. When the bed level decreases (net erosion), the content of the sub layer is equal to the previously defined content of the sub layer. Thus:

$$p_{i,J_{max}+1}^{n} = p_{i,J_{max}}^{n} \qquad u_z^n > 0$$
$$p_{i,J_{max}+1}^{n} = p_{i,sub}^{n} \qquad u_z^n < 0 \qquad (3.11)$$

The mixing coefficient is calculated by:

$$\Xi^n_{j+1/2} = D_b H\left[1-\frac{j\Delta z}{L_b}\right]+\alpha_p u_*^n d_{50} e^{-\frac{j\Delta z}{L_p}}$$
$$\Xi^n_{j-1/2} = D_b H\left[1-\frac{[j-1]\Delta z}{L_b}\right]+\alpha_p u_*^n d_{50} e^{-\frac{[j-1]\Delta z}{L_p}} \qquad (3.12)$$

3.3 Numerical apects

For solving the given equations in section 3.2 the time step and spatial step cannot be chosen arbitrarily, but these parameter are restricted by stability and accuracy conditions. The restrictions in the flow, sediment transport, bed level and bed composition model are discussed below.

3.3.1 Flow

In DELFT3D-FLOW the flow equations are solved by using the Alternating Direction Implicit method in the horizontal direction and a fully implicit integration in the vertical direction. An important dimensionless parameter for the behaviour of the flow solution is the Courant number:

$$\sigma_f = \sqrt{gH}\,\frac{\sqrt{2}\Delta t}{\sqrt{\Delta x \Delta y}} \qquad (3.13)$$

in which:
σ_f = Courant number for the flow [-]
Δx = spatial step in x-direction [m]
Δy = spatial step in y-direction [m]
Δt = time step [s]
g = gravitation acceleration [= 9.81 m/s^2]
H = water depth [m]

Because the solution method for the unsteady flow equations is implicit, no restrictions on the time step and spatial step are needed for stability. However, for accuracy the Courant number must be smaller than $4\sqrt{2}$ (Stelling, 1984).

3.3.2 Sediment transport

The suspended sediment transport equations are solved in the same way as the flow equations. The vertical direction is solved fully implicit, the horizontal directions are solved

by the Alternating Direction Implicit method. Therefore, the time step and spatial step are not restricted for stability.

For accuracy the Courant number must be smaller than $4\sqrt{2}$ (Stelling, 1984). The Courant number for suspended sediment transport is comparable to the Courant number for the flow in Eq. 3.13, but the propagation velocity is different. The propagation velocity for suspended sediment transport is about equal to the horizontal flow velocity (U) and thus much smaller than the propagation velocity for shallow waves ($\sqrt{gH}$). Therefore, the time step for solving the suspended sediment transport equation can be larger than for the flow equations. However, the time step for the solving the flow equations and the suspended sediment transport equations is equal in DELFT3D-FLOW.

The accuracy is also determined by the adaptation time and adaptation length of the sediment fraction. As a first approach, the depth-averaged adaptation time and length can be used for a three-dimensional computation. The depth-averaged adaptation time and length are given by:

$$T_i = \frac{H}{w_i} \qquad L_i = \frac{UH}{w_i} \tag{3.14}$$

in which:
T_i = Adaptation time for fraction i [-]
L_i = Adaptation length for fraction i [-]
w_i = Settling velocity for fraction i [m/s]
U = Depth-averaged velocity [m/s]
H = Water depth [m]

For accuracy the time and spatial step must be much smaller than the adaptation time and length scale.

3.3.3 Bed level

The bed level equation is solved explicitly. An upwind scheme is used for the bed load tranpsort fluxes and a central scheme for the suspended sediment transport. The time step for the bed level is generally restricted by the propagation velocity of bed level disturbances. However, no stability condition is presently derived for the bed level equation. During the numerical experiments, the time step is chosen sufficiently small in order to obtain a stable computation.

3.3.4 Bed composition

The bed composition is solved explicitly. Two dimensionless parameters are important for the maximum time and spatial step: the Courant number and the diffusion number (Vreugdenhil, 1989). Both parameters are given by:

$$\sigma_c = u_z \frac{\Delta t}{\Delta z} \qquad \lambda_c = 2\,\Xi \frac{\Delta t}{\Delta z^2} \tag{3.15}$$

in which:
σ_c = Courant number for the bed composition [-]
λ_c = Diffusion number for the bed composition [-]
Δt = Time step [-]
Δz = Spatial step [-]
u_z = Bed level velocity [m/s]
Ξ = Mixing coefficient [m^2/s]

By using the numerical scheme from section 3.2 the restriction for stability is as follows (Vreugdenhil, 1989):

$$\sigma_c^2 \le \lambda_c \le 1 \tag{3.16}$$

With increasing distance below the bed level, the mixing coefficient approaches zero. That indicates that the diffusion number (λ_c) also approaches zero for bed composition layers far below the bed level. Furthermore, the Courant number (σ_c) only depends on the bed level velocity and is constant for all bed composition layers. Thus, the stability condition cannot always be satisfied. Therefore, some artificial diffusion is added in Eq. 3.12 to keep the numerical computation stable.

For accuracy the time and spatial step are more restricted than for stability (3.16). When both parameters are much smaller than 1, the numerical computation is also accurate.

4 Case study: Noordelijk Deltabekken

4.1 Introduction

The estuary of the River Rhine and Meuse - the so-called 'Noordelijk Deltabekken'. - is situated in the western part of the Netherlands (Figure 4-1). After the flood in 1953 the 'Delta Plan' was developed to protect the south western part of the Netherlands against the sea. One part was the construction of the Haringvliet sluices at the mouth of the Haringvliet area (indicated by A in Figure 4-1). These sluices were built for both protection under high storm surge conditions as well as management of the navigation depth and salt intrusion in the Rotterdam harbour under low discharge conditions.

Figure 4-1 Noordelijk Deltabekken

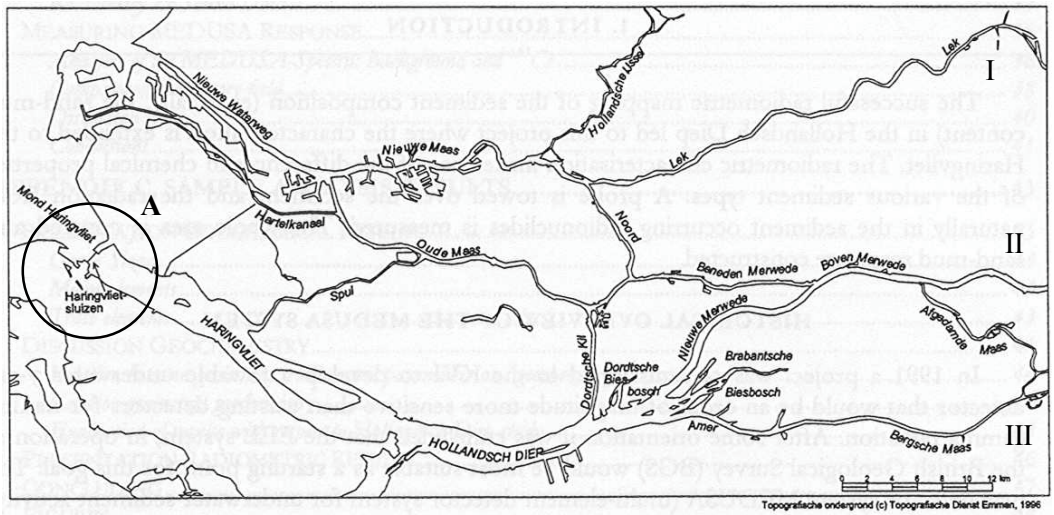

Due to the Haringvliet sluices, the water motion in the southern part of the Noordelijk Deltabekken (from west to east: Haringvliet, Hollandsch Diep, Nieuwe Merwede, Boven Merwede, Amer, Bergsche Maas) was completely changed (Figure 4-1). In the river branches Nieuwe Merwede and Bergsche Maas the tidal current changed into unidirectional flow under all discharge conditions. Furthermore, the maximum current velocities decreased significantly in the whole southern area. Due to these changes, an enormous amount of sand and mud deposited in this area and strong horizontal and vertical variations in the mud content are observed.

In the previous chapters, formulations (Chapter 2) and the numerical implementation (Chapter 3) of a morphological model were presented in which both sand and mud determine the bed level and composition development. In this chapter, the morphological model is applied to the southern part of 'Het Noordelijk Deltabekken'. First, the observed patterns of sand and mud deposition are described in more detail (4.2). Thereafter, the model set-up is discussed (4.3), the model results are presented (4.4) and the model

behaviour is analysed (4.5). Finally, the model results are compared with the observed sand-mud patterns in the southern area of the Noordelijk Deltabekken (4.6).

4.2 Sand-mud patterns

For the period 1971-1982 and 1982-1992 sediment balances were made for the whole 'Noordelijk Deltabekken' by Allersma (1988) and Van Dreumel (1995) respectively. The supply of sediment from the river branches Lek (indicated by I in Figure 4-1), Waal (II) and Meuse (III) for both sediment balances was estimated as follows:

Table 4-1 Annual supply of sand and mud (*10^9 kg/year)

	Sand		Mud	
Branch	**Allersma (1998)**	**Van Dreumel (1995)**	**Allersma (1988)**	**Van Dreumel (1995)**
Lek	0.8	0.30	0.5	0.55
Waal	1.3	1.05	2.3	2.40
Meuse	0.3	0.20	0.6	0.45

Based on field data (bed level and bed composition) and dredging data, Allersma (1988) calculated the amount of deposited/eroded sand and mud for each branch. For the southern area of the 'Noordelijk Deltabekken' the following estimations for the annual sand and mud deposition were made were for the period 1971-1982 (Table 4-2):

Table 4-2 Total deposition (+)/erosion (-) of sand and mud 1971-1982

Branch	**Sand (*10^9 kg)**	**Mud (*10^9 kg)**
Boven-Merwede	+2.86	+0.00
Nieuwe Merwede	+4.79	+2.05
Bergsche Maas	+0.70	+0.30
Amer	+3.14	+3.17
Hollandsch Diep (east)	+7.68	+1.92
Hollandsch Diep (west)	+3.27	+4.91
Haringvliet (east)	+0.96	+2.26
Haringvliet (west)	+1.50	+2.25

Van Dreumel (1995) divided the area in more sections for the sediment balance in the period 1982-1992. For the southern area of the 'Noordelijk Deltabekken' the following estimations for the annual sand and mud deposition were made were for the period 1982-1992 (Table 4-3):

Table 4-3 Annual deposition (+)/erosion (-) rate of sand and mud 1982-1992

Branch	Sand (*10^9 kg/year)	Mud (*10^9 kg/year)
Boven-Merwede	+0.257	+0.014
Nieuwe Merwede (north east)	+0.085	+0.015
Nieuwe Merwede (south west)	+0.002	+0.000
Bergsche Maas	+0.025	+0.006
Amer (east)	+0.017	+0.011
Amer (west)	+0.058	+0.086
Hollandsch Diep (east)	+0.030	+0.089
Hollandsch Diep (central)	+0.105	+0.421
Hollandsch Diep (west)	+0.050	+0.202
Haringvliet (east)	+0.044	+0.131
Haringvliet (central)	+0.041	+0.124
Haringvliet (west)	+0.030	+0.121

Visser (2000) concluded from field and dredging data in the Waal in the period 1970-1989 that the measured bed level changes could be explained by dredging activities only. A slight decrease in the bed level due to 'natural' erosion was estimated at 0.04 m.

Based on the data of Allersma (1988), Van Dreumel (1995) and Visser (2000) the deposition/erosion rates per unit area for both sand and mud are calculated for both periods 1971 - 1982 and 1982-1992. These are shown in Figure 4-2 and Figure 4-3. The total deposition/erosion rate per unit area is the sum of both sand and mud.

From these data the following remarks can be made about the morphological development and the distribution of sand and mud in this area:

- In the Waal and Bergsche Maas the morphological changes after the construction of the Haringvliet sluices were small for both periods compared with downstream areas.
- In the Boven-Merwede (both periods) and the north east part of the Nieuwe Merwede (1982-1992) the deposition rate is dominated by sand. Mud deposition does not play an important role in this area. However, in the Nieuwe Merwede (1971-1982) the mud deposition rate was about 30% of the total deposition rate.
- In the south west part of the Nieuwe Merwede (1982-1992) the morphological changes are very small due to the absence of sand and mud deposition.
- In the Amer both sand and mud are important for the total deposition rate during both periods.
- Between 1971-1982 the deposition rate in the eastern part of the Hollandsch Diep was dominated by sand while the deposition rate of mud was higher in the western part. In the Haringvliet area the annual mud deposition rate was slightly higher than the sand

deposition rate. Furthermore, the total deposition rates in the Haringvliet were significantly lower than in the Hollandsch Diep.

- The deposition in the Hollandsch Diep is dominated by mud in the period 1982-1992. Especially in the central area of the Hollandsch Diep the annual mud deposition rate is very high. For the same period the annual deposition rate in the Haringvliet area is also dominated by mud, but the annual deposition rate is significantly lower.

Figure 4-2 Deposition (+)/Erosion (-) rates per unit area for river branches 1971-1982

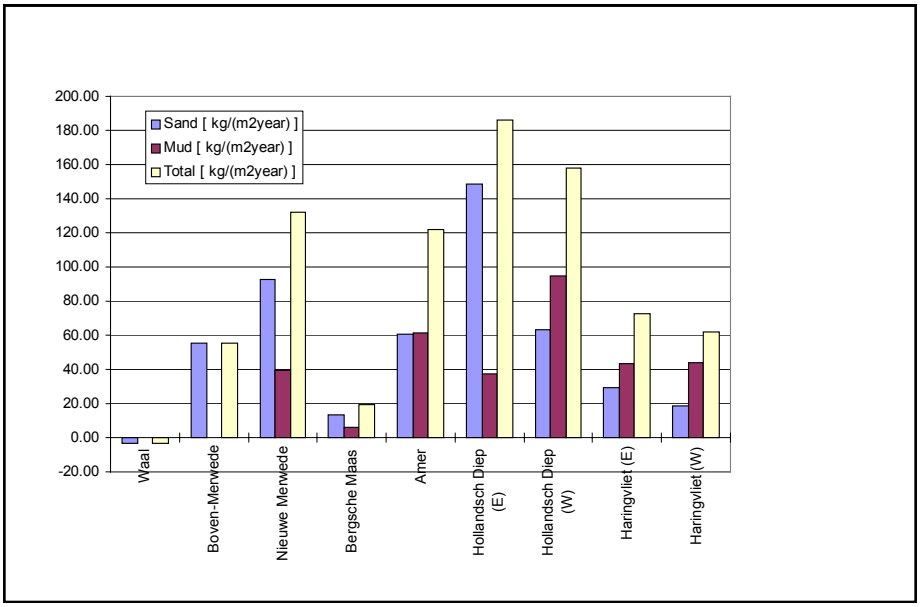

Figure 4-3 Deposition (+)/Erosion (-) rates per unit area for river branches 1982-1992

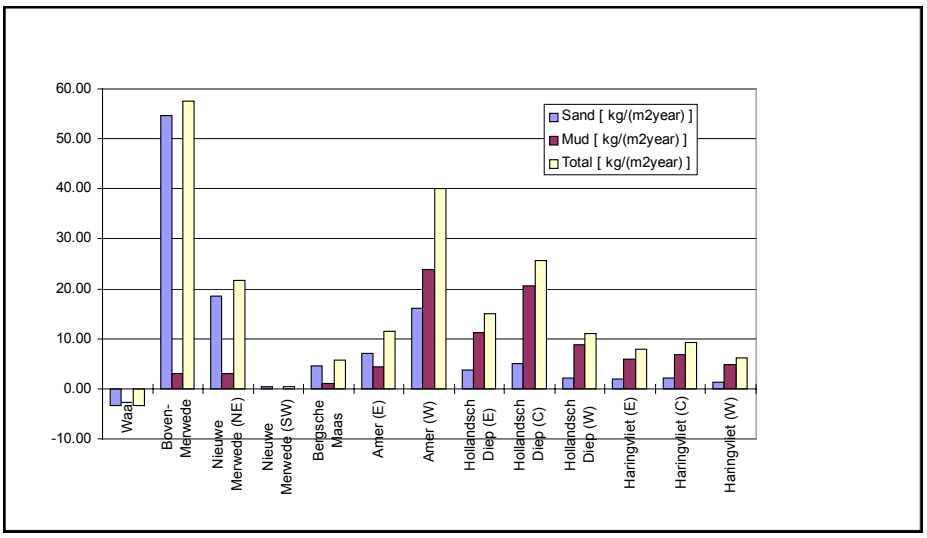

4.3 Model set-up

4.3.1 Introduction

The southern area of the Noordelijk Deltabekken is a very complex system. For example, the water motion is complex due to the management strategy of the sluices at the downstream side and the river discharge variations at the upstream side. Moreover, the system consists of two river branches at the upstream side and two channels in the Hollandsch Diep.

It is far beyond the present capabilities to start the model with the geometry existing in 1970 and compute the bed level and bed composition development with the measured boundary conditions at the upstream and downstream side. Therefore, the complexity of the geometry and the boundaries is strongly reduced. It is believed however that the large-scale characteristics can still be reproduced by the model.

4.3.2 Geometry

In first instance, a two-dimensional vertical approach (2DV) is chosen in order to understand the observed sand-mud patterns in longitudinal direction. Furthermore, the area is schematised as a one channel-system. About 81% of the yearly total load (sand & mud) at the boundary of the Hollandsch Diep is supplied by the Nieuwe Merwede (Van Dreumel, 1995). Therefore, the Amer and Bergsche Maas are neglected. The model set-up is representative for the branches Waal - Boven-Merwede - Nieuwe Merwede - Hollandsch Diep - Haringvliet.

In section 4.2 it was concluded that the morphological changes in the Waal due to the construction of the Haringvliet sluices were small compared to the downstream branches Boven-Merwede and Nieuwe Merwede. Therefore, the upstream boundary (subscript 0) is located near Tiel (about 100 kilometres upstream from the Haringvliet sluices) in the Waal ($x = 0$). The total length is set at $L_b = 100$ km. The downstream boundary (subscript 1) is located at the Haringvliet sluices ($x = L_b$).

4.3.3 Boundary conditions

At the upstream and downstream boundaries conditions are needed for the flow, the sediment transport and the bed level. In first instance all boundary conditions are chosen to be time-independent for reasons of simplicity.

At the upstream side, the flow is driven by a constant river discharge. The mean discharge of the Waal ($Q_0 = 1500$ m^3/s) is chosen to be representative. Furthermore, the equilibrium sand concentration at this boundary is used for the suspended sediment transport ($c_{s,0} = c_{s,eq}$). The mud concentration is prescribed at $c_{m,0} = 0{,}050$ kg/m^3 in order to reproduce the

total annual mud load of $2.4*10^9$ kg/year in the Waal (Table 4-1). Finally, it is assumed that the bed level does not change at the upstream boundary.

At the downstream side the tide is neglected and the water level is kept constant ($\zeta_1 = 0$). Thus, only outflow occurs at this boundary and weak boundary conditions are sufficient for suspended sand and mud transport. At this boundary the local derivative in space is set to zero ($\partial c_s/\partial x = 0$ and $\partial c_m/\partial x = 0$).

4.3.4 Bathymetry

Due to the 2DV approach the initial bed level cannot be approximated from measured depth soundings. In order to reproduce the current velocities in the whole area, the initial cross-sectional areas must be taken into account and translated into initial bed levels.

The cross-sectional area near Tiel is about 2000 m^2 and the width about 500 m. Near the Haringvliet sluices the cross-sectional area is about 20000 m^2. Compared with the water depth at Tiel the water depth at the Haringvliet sluices must be about 10 times larger to reproduce the cross-sectional area. The bed slope in the upstream river branch is estimated at about $i_{b,0} = 0.5*10^{-4}$. Finally, the bed roughness is kept constant in time and space. A Chézy-value of 50 $m^{1/2}/s$ is used.

Combining the discharge ($Q_0 = 1500$ m^3/s), the bed slope ($i_{b,0} = 0.5*10^{-4}$), the width ($B_0 = 500$ m) and the roughness ($C = 50$ $m^{1/2}/s$), the equilibrium water depth (h_e) and (depth-averaged) current velocity (u_e) can be estimated as follows:

$$h_e = \sqrt[3]{\frac{Q^2}{B^2 C^2 i_b}} \qquad u_e = C\sqrt{h_e i_b} \tag{4.1}$$

Thus, the equilibrium water depth $a_e \cong 4.16$ m and the equilibrium current velocity $u_e \cong 0.72$ m/s. The initial water depth at the Haringvliet sluices is then 41.6 metres. For the model area, it is assumed that the initial water depth adapts exponentially to the equilibrium water depth at the upstream side:

$$h(x) = h_e + (h_1 - h_e)e^{-\frac{L_b - x}{L_a}} \tag{4.2}$$

in which:
L_a = Adaptation length [m]
L_b = Basin length [m]
h_1 = Water depth at $x = L_b$ [m]
h_e = Equilibrium water depth [m]

An adaptation length of $L_a = 20000$ m is required in order to have a more or less equilibrium situation at the upstream side. The initial bed level is assumed to be equal to the equilibrium water level minus the initial water depth h(x):

$$z_b(x,t=0) = i_{b,0}(L_b - x) - h_e - (h_1 - h_e)e^{-\frac{L_b - x}{L_a}} \tag{4.3}$$

in which :
$i_{b,0}$ = Equilibrium bed level and water level slope [-]

4.3.5 Sediment parameters

Various sediment parameters must be prescribed for the sediment transport, the bed level and the bed composition. The parameter values are discussed below. It should be noted that these parameter values are for the reference computation. Several parameter values are also varied to analyse the sensivity of the model behaviour. The sensivity computations are discussed later on.

- **Sand grain size d_{50}**

The mean sand grain size is used for calculating the bed load transport rate and the reference concentration near the bed. This parameter is used to calibrate the total yearly sediment load for sand $V_{sand} = 1.05*10^9$ kg/year (dry weight) (Table 4-1).

In this area the mean sand grain size varies between 250 and 400 μm. For the calculation of the sediment transport rates the sediment transport formulas of Van Rijn are used. The total load is the sum of bed load and suspended load and can be calculated as follows:

$$S_t = S_b + S_s$$
$$S_b = 0.5 u_* d_{50} D_*^{-0.3} T \qquad S_s = \int_{z=a}^{z=h} u(z) c_s(z) dz \tag{4.4}$$

in which:
S_t = Total sediment load per unit width [m^2/s]
S_b = Bed load transport rate per unit width [m^2/s]
S_s = Suspended load transport rate per unit width [m^2/s]
u_* = Shear velocity [m/s]
d_{50} = Mean grain size [m]
D_* = Dimensionless grain size [-]
T = Transport parameter [-]
a = Reference height [m]
h = Water depth [m/s]
u(z) = Velocity at height z [m/s]
$c_s(z)$ = Sand concentration at height z [-]

For calculating the suspended transport rate, a logarithmic velocity profile for u(z) and a Rouse profile for c(z) is applied. For the reference concentration c_a the given expression in eq. 2.9 is used. By numerical integration, the suspended load transport (S_s) is obtained. Estimates of the bed load (S_b), suspended load (S_s), total load transport rate per unit width (S_t) are given as function of the grain size d_{50} in Table 4-4. The annual sediment load (V_s) is

obtained by multiplying the total load (S_t) with the sediment density (ρ_s = 2650 kg/m^3), width (B = 500 m) and time (3.15*10^7 s).

Table 4-4 Sediment transport rates and annual load for various grain sizes

Grain size (μm)	S_b (*10^{-5} m^2/s)	S_s (*10^{-5} m^2/s)	S_t (*10^{-5} m^2/s)	V_s (*10^9 kg/year)
200	0.6	4.1	4.7	1.97
300	0.7	1.7	2.4	1.00
400	0.9	1.1	2.0	0.83

From Table 4-4 it can be concluded that the bed load transport rate (S_b) slightly increases for increasing grain size. However, the suspended sediment load (q_s) strongly decreases with increasing grain size. Compared with the measured sediment load of V_s = 1.05*10^9 kg/year the calculated yearly sediment load for a grain size d_{50} = 300 μm (V_s = 1.00*10^9 kg/year) agrees rather well. This grain size is chosen for the reference computation.

- **Settling velocity sand and mud**

The settling time is directly related to the mean sand grain size (d_{50}) and given by w_s = 0.043 m/s. For this area an often used value for the settling velocity of mud is w_m = 0.5 mm/s. This value remains constant in time and space during the computation. It should be noted that flocculation is not taken into account.

- **Critical shear stress for erosion**

An overview of measurements showed that for natural beds in open water, the critical shear stress for erosion of a cohesive bed ($\tau_{e,c}$) ranges from 0.1 to 1.0 N/m^2 (Van Rijn, 1993). The large range is mainly explained by the consolidation process, which causes a time-dependency of the critical erosion shear stress. Herein, the consolidation process is not taken into account. Therefore, the critical erosion shear stress is constant in time and space. Less is known about the critical shear stress for mud particles of a non-cohesive bed ($\tau_{e,nc}$). In first instance, a constant value of 0.5 N/m^2 is used for the critical shear stress for erosion of mud particles from a non-cohesive bed ($\tau_{e,nc}$) and for erosion of a cohesive bed ($\tau_{e,c}$).

- **Erosion rate**

Measurements showed for natural beds in open water that the erosion rate (M) ranges from 1*10^{-3} to 1*10^{-5} kg/(m^{2}s). The range is mainly explained by the consolidation process. With a constant bed density (ρ_b = 1650 kg/m^3, see below), the erosion rate (M) is assumed to be M = 1*10^{-7} m/s.

- **Critical shear stress for deposition**

Measured values for the critical shear stress for deposition (τ_d) range from 0.05 - 0.25 N/m^2. Herein, a critical shear stress for deposition τ_d = 0.15 N/m^2 is used for the reference computation.

- **Critical mud content**

The transition between a non-cohesive and a cohesive behaviour occurs at a clay content (% < 2 μm) of about 5 - 10%. Often, a constant ratio between silt and clay is found in estuaries and therefore, a critical mud content can also be used. It is important to note that the critical mud content (p_{cr}) depends on the ratio between the silt and clay content in the area. However, no measurements are available to determine this ratio. Herein, the critical mud content is assumed to be $p_{cr} = 30\%$.

- **Bed density**

The bed density (ρ_b) is assumed to be constant in time and space. Herein, a constant value of $\rho_b = 1650$ kg/m^3 is used.

- **Mixing parameters**

For mixing within the bed no measured values are known. It is assumed that bioturbation does not play an important role. Thus, it is assumed that $\Xi_b = 0.0$ m^2/s. Furthermore, the (physical) mixing length is in the order of the bed forms and is assumed to be $L_m = 0.25$ m. The intensity parameter for the (physical) mixing process near the bed surface is assumed to be $\alpha_{m,p} = 0.0005$.

Table 4-5 Parameter values for reference computation

Parameter	Value	Unit	Parameter	Value	Unit
Q_0	1500	m^3/s	$\tau_{e,c}$	0.5	N/m^2
ζ_1	0.0	m	M	10^{-7}	m/s
C	50	m$^{1/2}$/s	τ_d	0.15	N/m^2
$c_{s,0}$	Equilibrium concentration		p_{cr}	0.30	[-]
$c_{m,0}$	0.050	kg/m^3	ρ_b	1650	kg/m^3
d_{50}	0.0003	m	Ξ_b	0.0	m^2/s
w_s	0.043	m/s	L_b	0.10	m
w_m	0.0005	m/s	$\alpha_{mix,p}$	0.0005	[-]
$\tau_{e,nc}$	0.5	N/m^2	L_p	0.25	m

Besides the reference computation several sensivity computations are being carried out. Because the morpological behaviour of this system is dominated by deposition only parameters are varied which determine the deposition of sand and mud significantly. The chosen parameters are the sand grain size (d_{50}), the critical shear stress for deposition (τ_d), the settling velocity for mud (w_m) and the mud concentration at the upstream boundary ($c_{m,0}$). An overview of the computations is given in Table 4-6.

Table 4-6 Overview of computations

Name	d_{50} [μm]	τ_d [N/m^2]	w_m [mm/s]	$c_{m,0}$ [mg/l]
Reference	300	0.15	0.50	50
DS200	***200***	0.15	0.50	50
DS400	***400***	0.15	0.50	50
TD005	300	***0.05***	0.50	50
TD025	300	***0.25***	0.50	50
WM100	300	0.15	***1.00***	50
WM025	300	0.15	***0.25***	50
CM075	300	0.15	0.50	***75***
CM025	300	0.15	0.50	***25***

4.3.6 Initial conditions

For the initial conditions the water levels, current velocities, sediment concentrations, bed level and bed composition must be prescribed. First, the computation is started without updating of the bed level and composition. When the current velocities, water levels and suspended sediment concentrations do not change anymore, the morphological computation is started. The initial bed level is already discussed in section 4.3.4. The initial bed composition is assumed to consist of sand without mud, i.e. the initial bed composition is equal to p_m (t = 0, x, y, z_c) = 0.0.

4.3.7 Numerical parameters

For the computation of the flow, sediment transport and bed level and composition, the grid size, the time step and the computation time must be defined (see also section 3.3). These parameters are discussed below.

- **Grid size**

The grid size in horizontal direction is taken Δx = 500 m. In the water column, ten layers (k_{max} = 10) are assumed to be sufficient. In the water column the grid size is not constant, but depends on the water depth. A logarithmic distribution is assumed and the cell at the bed is assumed to be 2% of the water depth. The grid size for the bed composition is Δz = 0.1 m. Forty layers are used for the bed composition computation (J_{max} = 40).

- **Time step**

For the computations of flow, sediment transport and the bed level and bed composition various restrictions can be given for the time step (see also section 3.3).

The time step for the flow is restricted by the propagation velocity of shallow waves. The maximum water depth is assumed to be 40 metres. The propagation velocity is then about equal to 20 m/s. The Courant number (σ_f) must be smaller than about 10. The time step is chosen $\Delta t = 60$ s. For this time step the Courant number is about equal to 2.

The time step for the suspended sediment transport is restricted by the settling time of a particle from the water surface to the bed. Because the settling time of a sand particle is much smaller than for a mud particle, sand transport in suspension determines the time step. By using h = 4 metres, $w_s = 0.04$ m/s and u = 1 m/s the settling time is estimated at $T_s = 100$ s and the settling length at $L_s = 100$ m. This is larger than the chosen time step for the flow ($\Delta t = 60$ s) and initially assumed to be sufficient for accuracy. The length scale for suspended sand is much smaller than the grid size ($\Delta x = 500$ m). Therefore, the computation of the suspended sediment concentration will not be very accurate, but it is assumed to be sufficient in first instance.

The time step for the bed level and bed composition is generally much larger than for the flow and the suspended sediment transport. For the bed level the propagation velocity of a bed disturbance restricts the time step. As a first approximation, the time step for the bed level can be calculated by using the total sediment load for sand $s = 5*10^{-5}$ m^2/s, the water depth h = 4 m, the transport coefficient n = 5 [-] and the bed porosity $\varepsilon_p = 0.4$. The propagation velocity for sand only is about equal to $6.7*10^{-5}$ m/s ($\cong$ 5.8 m/day). The Courant number for the bed level equals 1 for a time step $\Delta t = 86$ days.

For the bed composition computation two dimensionless parameters are imporant for the time step (see section 3.3.4): the Courant number (σ_c) and the diffusion number (λ_c). For accuracy the diffusion number must be much smaller than 1 and it is chosen to be 0.1. The mixing coefficient can be estimated by using reasonable values for the shear velocity (u_*) and the grain size (d_{50}). The maximum mixing coefficient is estimated by $\Xi_m = 0.5*10^{-8}$ m^2/s. By using the grid size in the bed ($\Delta z = 0.10$ m), the maximum time step equals $\Delta t =$ 100 000 s ($\cong$ 28 hours). By using the total sediment load for sand $s = 5*10^{-5}$ m^2/s, the grid size in horizontal direction and the bed porosity $\varepsilon_p = 0.4$, the propagation velocity of the bed level (u_z) is about equal to $1.7*10^{-7}$ m/s ($\cong$ 0.01 m/day). The square of the Courant number for the bed level must be smaller than the diffusion number. The Courant number is assumed to be 0.05. Thus, $\Delta t = 30\,000$ s ($\cong$ 8.3 hours). This time step is the most restricting time step for the bed level and composition computation and therefore chosen for the bed level and bed composition computation.

Compared to the time step of the flow calculation ($\Delta t = 60$ s), the time step for the bed level and composition ($\Delta t = 30\,000$ s) is much larger. The ratio between the latter and the former time step is called the morphological factor (N_{morf}). So, herein $N_{morf} = 500$ is applied.

Because the mixing coefficient decreases with increasing distance below the bed level, the stability condition cannot be fulfilled for bed composition far below the bed level (see section 3.3.4). Therefore, a small artifical mixing coefficient (Ξ_{num}) is added to the mixing coefficient to keep the numerical computation stable. The artificial mixing must be small

with respect to the maximum mixing coefficient (Ξ_{mix} = 1*10^{-8} m^2/s) and set to Ξ_{num} = 1*10^{-10} m^2/s.

- **Simulation time**

The simulation time must be at least twenty years to compare the results with the presented sediment balances for the periods 1971-1982 and 1982-1992 in section 4.2. Moreover, the time scale needed to fill the whole basin with sand and mud must also be considered for the choice of the computation time. This time scale can be estimated as follows. The total inflow of sediment (sand and mud) from upstream is about 3*10^9 kg/year. The total volume which is filled with sand and mud can be estimated by integrating the difference between the equilibrium depth and the initial depth at time t = 0. The initial depth is given by:

$$h(x) = h_e + (h_1 - h_e)e^{-\frac{(L_b - x)}{L_a}} \tag{4.5}$$

in which:
h_1 = Water depth at mouth [m]
h_e = Equilibrium water depth upstream [m]
L_b = Basin length [m]
L_a = Adaptation length of water depth [m]

Integrating the difference between the initial water depth and the equilibrium water depth over the total distance of the basin L_b gives the total area per unit width which is filled with sand and mud:

$$A = L_a(h_1 - h_e)\left[1 - e^{-\frac{L_b}{L_a}}\right] \tag{4.6}$$

in which:
A = Area to be filled with sand and mud [m^2]

By using L_a = 20000 m, h_1 = 40 m, h_e = 4.16 m, L_b = 100000 m and the width B = 500 m, the total volume to be filled is equal to 3.6*10^9 m^3. By using the bed density ρ_b = 1650 kg/m^3 the total amount of sediment required to fill the whole basin is equal to 6*10^{11} kg. Comparing the required volume of sediment (6*10^{11} kg) to the yearly supply of sediment at the upstream boundary (3*10^9 kg), an estimation of the total time needed to fill the whole basin is about 200 years.

The simulation time is set to 50 years for all computations in order to have a reasonable computation time on a stand-alone PC. It is expected that significant morphological behaviour can be observed during this period. Moreover, the results can also be compared with the sediment balances in the first twenty years after the construction of the Haringvliet sluices. One extra computation with the reference settings is being carried out with a simulation time of 150 years (denoted as: Reference+).

4.4 Results

The computation time of a 50 year simulation at a stand-alone PC (450 MHz, 64.0 MB RAM) was about 6 hours for each computation. The following variables were dynamically computed:

- water level (ζ)
- velocities (u, v, w)
- concentrations (c_s, c_m)
- bed level (z_b)
- mud content in the bed (p_m)

In Appendix A these variables are shown in three figures for time intervals of ten years for each computation. The figure numbers of the accompanying computations are given in Table 4-7.

Table 4-7 Overview of computations

	Parameters				Figures
Name	**d_{50} [μm]**	**τ_d [N/m^2]**	**w_m [mm/s]**	**$c_{m,0}$ [mg/l]**	**Appendix A**
Reference	300	0.15	0.50	50	4.1 - 4.3
DS200	***200***	0.15	0.50	50	4.4 - 4.6
DS400	***400***	0.15	0.50	50	4.7 - 4.9
TD005	300	***0.05***	0.50	50	4.10 - 4.12
TD025	300	***0.25***	0.50	50	4.13 - 4.15
WM100	300	0.15	***1.00***	50	4.16 - 4.18
WM025	300	0.15	***0.25***	50	4.19 - 4.21
CM075	300	0.15	0.50	***75***	4.22 - 4.24
CM025	300	0.15	0.75	***25***	4.25 - 4.27
Reference+	300	0.15	0.50	50	4.28 - 4.30

In these figures, the following is shown respectively:

- First figure: the water level (a), the water depth (b), bed shear stress (c), depth-averaged sand (d) and depth-averaged mud concentration (e) along the basin. The horizontal axis is the distance along the basin. It is made dimensionless with the basin length L_b.
- Second figure: the bed level changes due to sand deposition (a), the bed level changes due to mud deposition (b), the mud content at the bed surface (c), the mean mud content in the active layer (d) and the bed level (e) along the basin. The horizontal axis is the distance along the basin. It is made dimensionless with the basin length L_b.
- Third figure: the mud content in the active bed layer is shown for $x/L_b = 0.60$ (a), $x/L_b = 0.70$ (b), $x/L_b = 0.80$ (c), $x/L_b = 0.90$ (d) and $x/L_b = 1.00$ (e). At the vertical axis the bed level is shown. The reference level is the initial bed level at each location.

With respect to the Reference computation results the following remarks can be made (Figure 4.1, 4.2 and 4.3 in Appendix A):

- For each time step the water level (Figure 4.1a) has a more or less constant slope for $x/L_b < 0.5$ and is almost equal to the downstream water level for $x/L_b > 0.5$. The water level slope in the upstream area ($x/L_b < 0.6$) decreases in time.
- The initial bed shear stress (Figure 4.1c, t = 0 years) along the basin is about constant for $x/L_b < 0.4$. Hereafter, the bed shear stress decreases gradually towards the downstream boundary of the basin. For the other time steps, the bed shear stress shows an steep front which propagates in downstream direction.
- Two areas can be distinguished for which the bed level increases in time due to deposition of sand and/or mud (Figure 4.2a, 4.2b, 4.2e). These areas are denoted as area 1 ($0.4 < x/L_b < 0.6$) and area 2 ($0.66 < x/L_b < 1.0$). From 4.2a and 4.2b it can be observed that the bed level changes in area 1 are caused by sand deposition, the bed level in area 2 raises due to mud deposition.
- The deposition wave for sand (Figure 4.2a) can be characterised as a propagating 'shock' wave. The bed level changes due to sand deposition increase very gradually, reaching a maximum and then decrease very rapidly towards zero. Furthermore, the propagation velocity of the maximum decreases in time. At time t = 10 years a small jump is observed at the front of the sand wave. This jump disappears after some time and does not seem to influence the computation later on.
- The deposition wave for mud (Figure 4.2b) has a different form compared to the sand wave (Figure 4.2a). An onset for mud deposition is observed at $x/L_b = 0.66$. Upstream of this point no bed level changes due to mud deposition occur. The bed level changes due to mud increase from the onset towards a certain maximum and then decrease gradually towards the end of the basin. The maximum bed level change due to mud deposition propagates in downstream direction.
- The mud content at the bed surface (Figure 4.2c) is zero beyond the onset of mud deposition ($x/L_b = 0.66$). Hereafter, the mud content increases, reaches a maximum and then decreases again. After 20 years the mud content at the bed surface reaches 100%. However, the area around the downstream boundary still remains very sandy. The same yields for the mean mud content in the whole active layer (Figure 4.2d).
- In Figure 4.3 the mud distribution within the bed is shown. The bed level on the vertical axis is relative to the initial bed level. For $x/L_b = 0.6$ the bed composition remains sandy, because this location is upstream from the onset of mud deposition ($x/L_b = 0.66$).Due to sand deposition the computational grid for the bed composition shifts upward about 4 metres. For the other locations the mud distribution in the bed (Figure 4.3b - 4.3e) is strongly stratified. The upper layer (above z = 0) is dominated by mud, while the lower layer (below z = 0) mostly consists of sand.

The other computations are compared with the reference computation only. The following remarks can be made:

- Computation DS200 shows that the bed level changes due to sand deposition are significantly higher (Figure 4.5a). Furthermore, the propagation velocity of the sand wave first decreases but then increases again when it reaches the area of mud deposition.
- Computation DS200 also shows that the mud content at the bed surface has the same characteristics compared with the reference computations (Figure 4.5c). The bed in the

mud deposition area ($x/L_b > 0.65$) changes into a muddy area. After 30 years, the mud in the exchange layer becomes sandy again. This can also be observed in the mean mud content in the whole active layer (Figure 4.5d).

- Compuation DS400 shows the same patterns as computation DS200, but the bed level changes due to sand and the propagation velocity of the sand wave are much smaller (Figure 4.8a). Moreover, a more pronounce jump in the bed level changes due to sand is observed which remains during the whole computation.
- In computation TD005 it can be observed that the onset of the mud deposition area shifts in downstream direction and is equal to $x/L_b = 0.78$ (Figure 4.11b). For computation TD025 the onset shifts in upstream direction and is equal to $x/L_b = 0.61$ (Figure 4.14b). The form of the deposition waves also changes. For TD005 the maximum bed level change due to mud is about 5 000 m downstream from the onset of mud deposition at time t = 10 years (Figure 4.11b). TD025 shows that the same maximum is about 10 000 m downstream from the onset (Figure 4.14b).
- Computation WM025 (Figure 4.16 - 4.18) and WM100 (Figure 4.19 - 4.21) show that the decrease of the suspended mud concentration along the basin is significantly affected by the settling velocity. For a lower settling velocity the mud concentration decrease is smaller and vice versa (Figure 4.16e and Figure 4.19e respectively). Figure 4.17b and Figure 4.20b also show that the bed level changes due to mud are also different. For a higher settling velocity the mud deposition wave has a very pronounced maximum (4.20b), while for a lower settling velocity the mud wave is much flatter (Figure 4.17b).
- Computations C075 and C025 both show that the bed level changes due to mud are strongly affected by the upstream mud concentration. For C075 (Figure 4.23b) and C025 (Figure 4.26b) the bed level changes are considerably higher and lower respectively. The onset and the form of the deposition wave do not seem to be affected by the upstream boundary concentration.

With respect to the Reference+ simulation (Simulation time 150 years instead of 50 years, other physical and numerical parameter values equal to Reference computation) the following remarks can be made (Appendix A: Figures 4.28 - 4.30):

- It can be observed that the water depth tends towards the equilibrium water depth (Figure 4.28b). The bed shear stress (Figure 4.28c) and the depth-averaged sand concentration (Figure 4.28d) along the basin become more and more uniform. The same yields for the mud concentration (Figure 4.28e). After 150 years, the mud concentration along the basin is almost everywhere equal to the mud concentration at the upstream boundary.
- The sand wave and mud wave are both propagating in downstream direction (Figure 4.29a and Figure 4.29b respectively). Moreover, the initial mud deposition area is covered with sand after some time (Figure 4.29e). After 150 years, the downstream area is still not adapted to the new equilibrium (Figure 4.29e).

The various observed characteristics are analysed further in the next section.

4.5 Analysis

The results in section 4.4 showed two characteristic morphological phenomena: the propagating sand wave and the propagating mud wave. By applying some approximations these phenomena can be described by analytical solutions. The advantage of analytical solutions is that these give a lot of physical insight in the behaviour of the model. In this section the observed sand and mud wave are discussed subsequently.

4.5.1 Sand wave

The reference computation (d_{50} = 300 μm), DS200 (d_{50} = 200 μm) and DS400 (d_{50} = 200 μm) show a propagating sand wave. The following characteristics were observed:

- The propagation velocity decreases in time;
- The propagation velocity decreases with increasing sand grain size;
- The propagation velocity increases again when the mud deposition area is reached;
- The sand wave has a steep front;

This behaviour can be explained as follows:
The adaptation length of sand in suspension is relatively small compared with the horizontal grid size. With a settling velocity of about 0.04 m/s, a depth-averaged velocity of 1 m/s and a water depth of 7.5 m, the adaptation length is about 150 metres, while the horizontal grid size is 500 metres. A small adaptation length scale compared with the grid size means that the sand concentration almost instantaneously adapts to the equilibrium value.

At the upstream side of the basin ($x/L_b < 0.2$) the total transport rate of sand (bed load and suspended load) is nearly uniform due to the uniform bed shear stress in this area. Therefore, the bed level is about constant in time. Further downstream the water depth increases and the velocity decreases. The total sand transport rate also decreases and the bed level increases in time due to the horizontal gradient in the total sand transport rate. The bed level rise continues until the total sediment transport rate is equal to the total transport rate upstream. This implicates that the initial water depth decreases until it is equal to the equilibrium water depth. Thus, the propagation velocity of the sand wave depends on the ratio between the sediment transport capacity and the difference between the initial (Eq. 4.2) and equilibrium water depth. The propagation velocity can be approximated by:

$$c_{b,s} = \frac{s}{(h_1 - h_e)e^{-\left(\frac{L_b - x}{L_a}\right)}} \tag{4.7}$$

in which:
$c_{b,s}$ = Propagation velocity of sand wave [m/s]

From this equation it can be seen that the propagation velocity of the sand wave decreases in downstream direction because the difference between the equilibrium water depth and the actual water depth increases. Furthermore it can be observed that the propagation

velocity strongly increases with decreasing grain size (d_{50}), because the total sand transport rate (s) increases with decreasing grain size (see also Table 4-4). Moreover, when the sand wave reaches the mud deposition area the propagation velocity increases because the initial water depth is already decreased by mud deposition.

4.5.2 Mud wave

The mud wave has the following characteristics:

- At a certain distance from the upstream boundary mud deposition starts. The onset differs for different values of the critical shear stress for deposition.
- Beyond the onset, the mud concentration decreases and approaches zero. The decrease depends on the settling velocity and the critical shear stress for deposition. When the settling velocity and/or the critical shear stress is higher, the decrease in the mud concentration beyond the onset is larger.
- Beyond the onset, the bed level changes due to mud first increase, reach a maximum at a certain distance beyond the onset and then decrease again. The form of the mud wave depends on the settling velocity and the critical shear stress for deposition. When the critical shear stress for deposition and the settling velocity for mud are higher, the maximum is more pronounced.
- When the upstream mud concentration is higher, the bed level changes due to mud are also larger and vice versa.

This behaviour can be explained as follows:

- **Onset of mud deposition**

The onset of mud deposition (x_d) can be approximated by (Appendix B.1):

$$\frac{x_d}{L_b} = 1 + \frac{L_a}{L_b} \ln \left(\frac{\frac{h_d}{h_e} - 1}{\frac{h_1}{h_e} - 1} \right) \tag{4.8}$$

in which:

x_d = Onset of mud deposition [m]
L_b = Basin length [m]
L_a = Adaptation length of initial bed level profile [m]
h_d = Critical water depth for deposition [m]
h_e = Equilibrium water depth [m]
h_1 = Initial water depth at boundary $x = L_b$ [m]

The critical water depth (h_d) is the water depth at which mud deposition starts and is equal to the ratio between the discharge per unit width (q) and the (depth-averaged) critical velocity for deposition (u_d). By using (4.8) and $q = 3$ m^2/s, $h_e = 4.16$ m, $L_a = 20\,000$ m, $L_b = 100\,000$ m, $h_1 = 41.6$ m, the critical water depth (h_d) and the onset of mud deposition relatively to the basin length (x_d/L_b) are given in Table 4-8 for various values of the critical deposition shear stress (τ_d). The numerical results are given in the last column.

Table 4-8 Critical water depth and onset for mud deposition

	τ_d (N/m^2)	u_d (m/s)	h_d (m)	Analytical x_d/L_b (-)	Numerical x_d/L_b (-)
Reference	0.15	0.29	10.3	0.64	0.66
TD005	0.05	0.17	17.6	0.80	0.78
TD025	0.25	0.38	7.9	0.54	0.61

Comparing the results indicates an agreement between the analytical and numerical solutions. It is obvious that for decreasing critical shear stress the onset shifts in the downstream direction, because the water depth must be larger for a smaller flow velocity.

- **Mud concentration and bed level changes**

By assuming a horizontal water level and a linear bed slope beyond the onset of mud deposition, the initial mud concentration (c_m), the initial mud deposition rate (D) and the initial distance of the maximum deposition rate relatively to the onset (x_m) can be approximated as follows (see also Appendix B.2 and B.3):

$$c_m(x) = c_{m,0} e^{-\frac{1}{L_m}\frac{x^2}{(L_d+x)}} \tag{4.9}$$

$$D(x) = w_m c_{m,0} e^{-\frac{1}{L_m}\frac{x^2}{(L_d+x)}} \left[1 - \frac{1}{\left(1+\frac{x}{L_d}\right)^2} \right] \tag{4.10}$$

$$x_m = \frac{1}{2}\sqrt{2}\sqrt{L_d L_m} \tag{4.11}$$

in which:
L_m = Adaptation length settling mud [m]
L_d = Adaptation length flow [m]
x = Distance from onset of mud deposition [m]
w_m = Settling velocity mud [m/s]
$c_{m,0}$ = Mud concentration at x = 0 [-]
D = Deposition rate [m/s]
x_m = Distance of maximum deposition rate relatively to onset x_d [m]

In the analytical expressions for the mud concentration (4.9) and mud deposition (4.10) two length scales can be observed. These length scales L_m and L_d are given by:

$$L_m = \frac{q}{w_m} \qquad L_d = \frac{q}{u_d i_{b0}} \tag{4.12}$$

in which:
u_d = Critical deposition velocity [m/s]
i_{b0} = Initial bed slope [-]
u_d = Critical depth-averaged velocity for mud deposition [-]

By using (4.9) and (4.10) the concentration (c_m) and the deposition rate (D) are computed for the reference computation, WM025 and WM100. For these computations the length scales L_d and L_m and the distance of the maximum for mud deposition (x_m) relatively to the onset (x_d) are as follows:

Table 4-9 Length scales and distance of the maximum mud deposition

	w_m [mm/s]	L_m [m]	h_d [m]	i_{b0} [-]	L_d [m]	x_m [m]
Reference	0.5	6000	10.3	0.0009	11200	5800
WM100	1.0	3000	10.3	0.0009	11200	8200
WM025	0.25	12000	10.3	0.0009	11200	4100

In Figure 4-4 the mud concentration in the water column along the basin after five years is shown by using the analytical expression (eq. 4.9, solid symbols) and the numerical results for the reference computation, WM100 and WM025 (open symbols). The mud concentration at the vertical axis is given relatively to the concentration at the upstream boundary ($c_{m,0}$).

Figure 4-4 Mud concentration along the basin

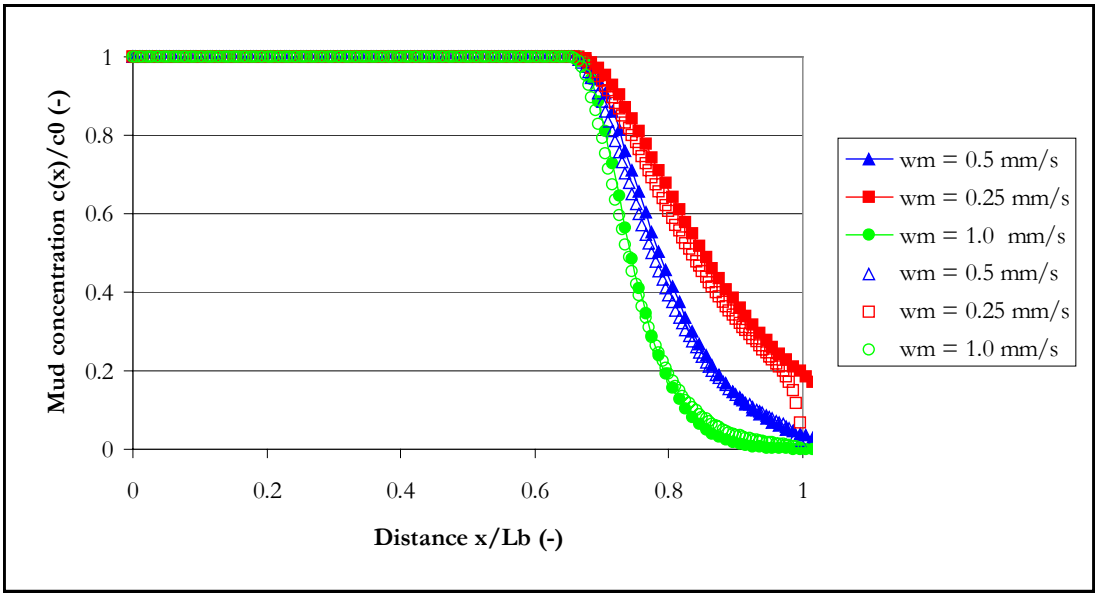

In Figure 4-5 the bed level change due to mud deposition after five years is shown by applying the analytical expression for the mud deposition rate (eq. 4.10, solid symbols) and

the numerical results for the reference computation and WM100 and WM025 (open symbols).

Figure 4-5 Mud deposition along the basin after five years

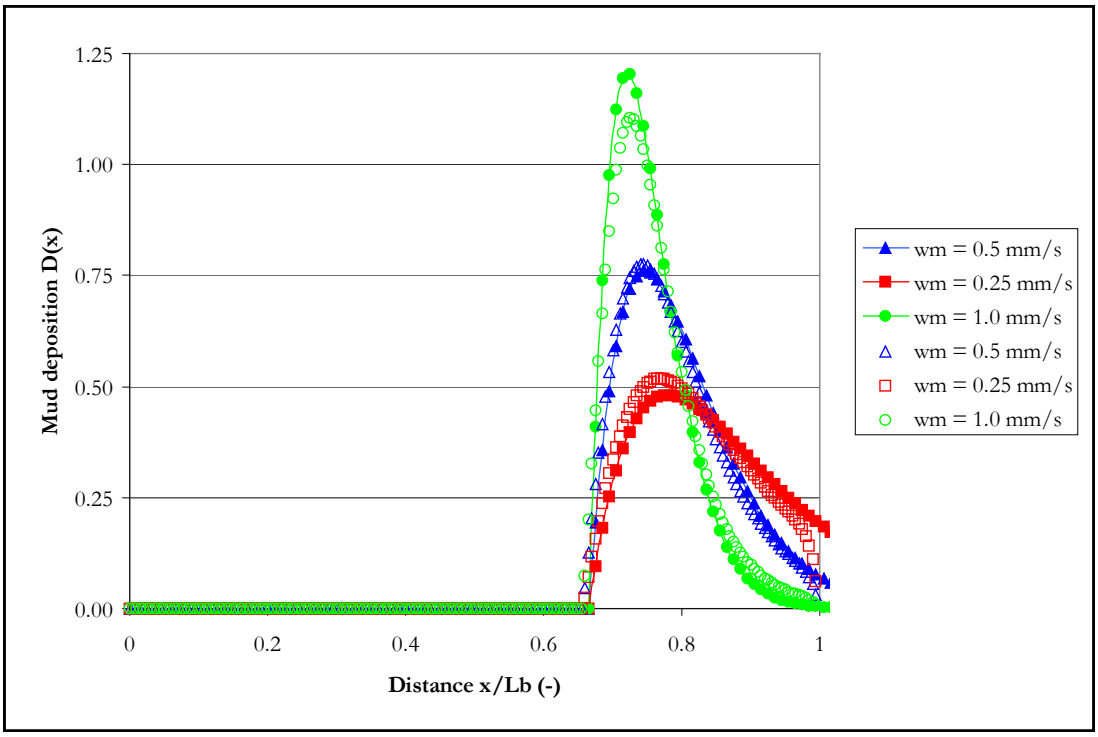

It should be noted that for both the mud concentration and the mud deposition the numerical result for the onset of mud deposition (x_d) is used instead of the analytical expression (4.8).

From Figure 4-4 and Figure 4-5 it can be concluded that the analytical expressions agree well with the numerical results. Thus, the derived expressions can be used for explaining the behaviour.

In the analytical expressions for the mud concentration (4.9) and mud deposition (4.10) two length scales are important (4.12). The first length scale (L_m) expresses the distance in which mud settles from the water surface to the bed. When the setting velocity (w_m) increases, the length scale (L_m) decreases and vice versa. This length scale is equal to the well-known adaptation length scale for suspended sand. However, the adaptation length scale for mud is generally much larger than for sand.

The second length scale (L_d) contains the ratio between the discharge per unit width (q) and the critical velocity for deposition (u_d). This ratio is the water depth at the onset of mud deposition: the so-called critical water depth (h_d). The length scale L_d expresses the distance from this point in which the water depth becomes two times larger than the critical water depth (Figure 4.6). In other words: the length scale L_d expresses the distance from the onset of mud deposition in which the depth-averaged flow velocity becomes two times smaller than the critical flow velocity for deposition (u_d).

It is easy to observe that when the bed slope (i_{b0}) is very small (i.e. the water depth increases very slowly with respect to the critical water depth), the flow velocity decreases

very slowly and the length scale L_d is very large. Moreover, the length scale L_d also increases when the critical velocity for deposition decreases.

Figure 4-6 Length scale L_d

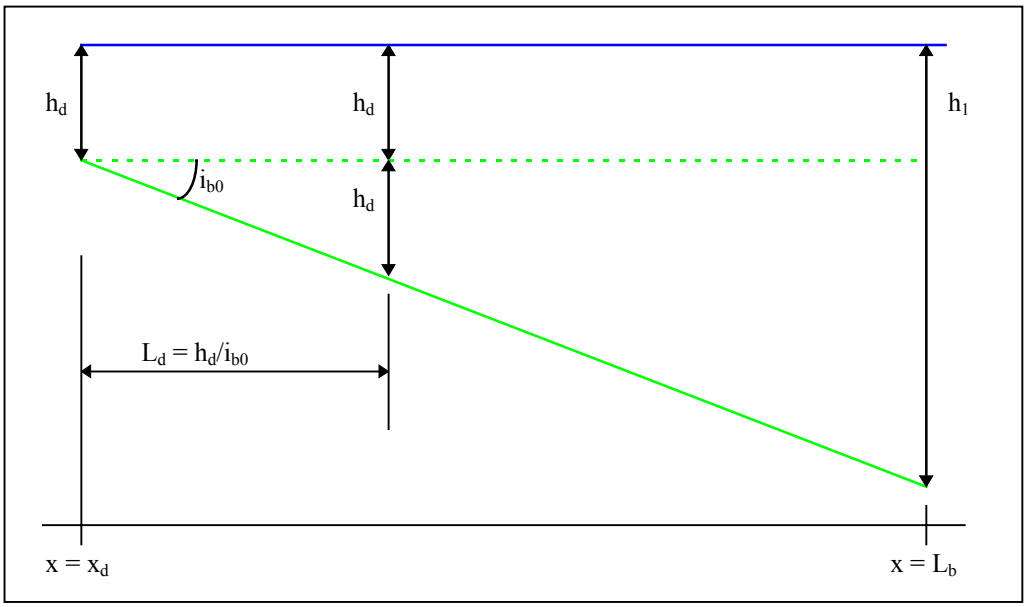

By using these length scales the mud concentration (Figure 4-4) and the bed level changes due to mud (Figure 4-5) can be explained as follows:

From (4.9) it can be seen that the mud concentration always decreases in downstream direction and approaches zero for large x. Both length scales (L_m and L_d) play a role. For increasing length scales (and thus for decreasing settling velocity (w_m) and critical velocity for deposition (u_d)) the decrease in mud concentration is less sharp. This is also observed in the numerical results.

For the reference computation, WM100 and WM025 only L_m varies (Table 4-9). The stronger decrease in the mud concentration for WM100 compared with the reference concentration can be explained by the smaller length scale L_m. Due to the larger settling velocity the mud concentration decreases faster. For WM025 the settling velocity is smaller (L_m larger) and the decrease in the mud concentration decrease is less sharp.

From (4.10) it can be seen that the bed level changes due to mud are zero at the onset and approach zero a long way from the onset. From (4.11) it can be observed that the position of the maximum mud deposition rate depends on both length scales L_m and L_d.

For the reference computation, WM100 and WM025 only L_m varies (Table 4-9). The more pronounced bed level change due to deposition in WM100 compared with the reference concentration can be explained by the smaller settling length scale L_m. The smaller settling length scale also causes that the maximum mud deposition rate lies closer to the onset. For WM025 the settling velocity is smaller (L_m larger) and the maximum is less pronounced and lies further downstream of the onset.

From these analytical expressions two areas can be distinguished downstream from the onset of mud deposition. The amount of mud deposition just beyond the onset (x_d) is mainly limited by the second term in (4.10) in which the length scale L_d plays an important role.

The mud deposition is small because the flow velocity is about equal to the critical velocity for deposition. Mud deposition in this area is called 'flow limited'. Downstream from the maximum mud deposition rate, mud deposition is limited because the suspended mud concentration in the water column (c_m) is very low. Mud deposition in this area is called 'supply limited'. In the area between both the flow velocity and the mud concentration in the water column are low respectively high enough for reaching a maximum mud deposition rate.

4.6 Discussion

Finally the computational results shown in section 4.4 and the analysis in section 4.5 are used for discussing the observed sand-mud patterns in the Noordelijk Deltabekken (section 4.2). It should be noted that the model is set-up with realistic values for the sections Waal - Beneden-Merwede - Nieuwe Merwede - Hollandsch Diep - Haringvliet. Due to various simplifications the sand-mud patterns are only qualitatively discussed for this area.

In Figure 4-2 and Figure 4-3 the deposition and erosion rates of sand and mud are shown for the area of interest in the periods 1971-1982 and 1982-1992 respectively (see section 4.2). In Figure 4-7 the computed bed level changes due to sand and mud deposition after ten and twenty years are given for the reference computation only. The locations of the sections Waal (WL) - Boven-Merwede (BM), Nieuwe Merwede (NM), Hollandsch Diep (HD) and Haringvliet (HV) are also indicated in Figure 4-7.

Figure 4-7 Computed bed level changes for reference computation

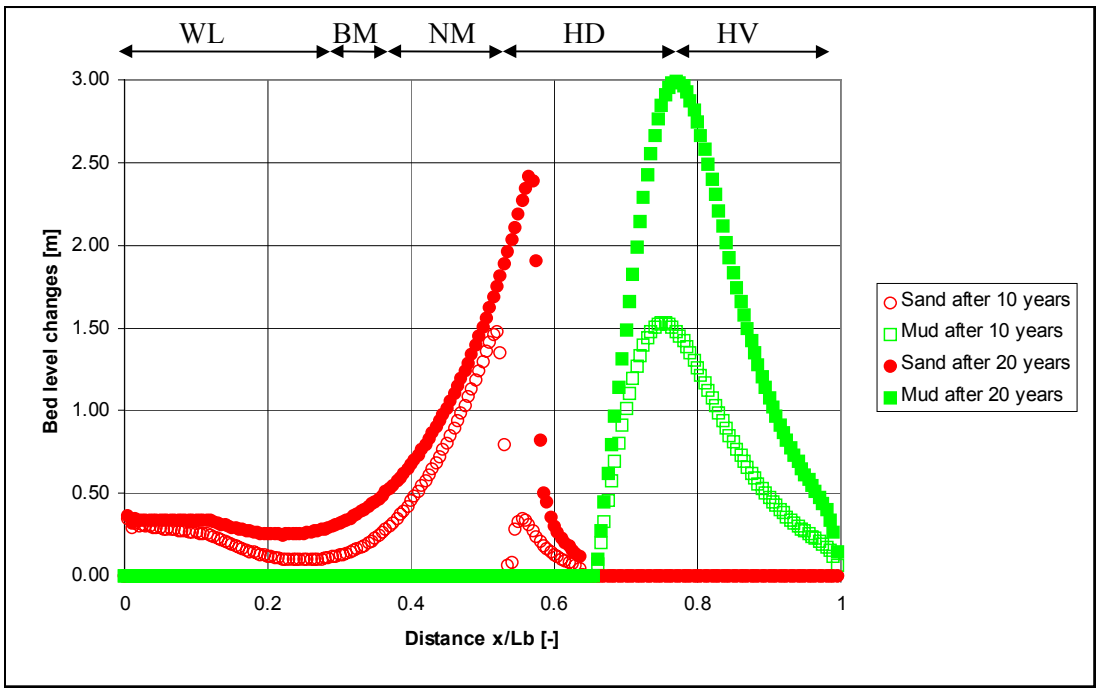

By comparing the field data and the computational results the following remarks can be made:

- The model results suggest two deposition areas in the first twenty years after the construction of the Haringvliet sluices (Figure 4-7): a sand deposition area in the

upstream areas and mud deposition area more downstream. Especially in the period 1982-1992 (Figure 4-3) this pattern is also observed in the field data. On the one hand, the Boven-Merwede and Nieuwe Merwede were dominated by sand deposition. On the other hand, mud deposition was dominant in the Hollandsch Diep and Haringvliet area. However, this pattern is less clear in the period 1971-1982 (Figure 4-2).

- The model results show a travelling sand wave in downstream direction. The field data does not correspond with this pattern. In the period 1971-1982 the maximum sand deposition is in the eastern section of the Hollandsch Diep, while the same maximum is in the Boven-Merwede more upstream from the Hollandsch Diep in the period 1982-1992.
- The model results also show that downstream from the sand deposition area no deposition of sand occurs because the supply of sand is zero. The field data however suggest that there is still an amount of sand which is deposited in the Hollandsch Diep and in the Haringvliet area for both periods.
- A zone without sand and mud deposition between the aforementioned deposition areas of sand and mud is observed in the model results. For the period 1982-1992 the south west part of the Nieuwe Merwede probably shows this behaviour. Sand and mud deposition were both very small compared with upstream and downstream areas. In the period 1971-1982 an area with significantly less deposition between the sand and mud deposition areas cannot be distinguished.
- A characteristic mud deposition pattern is obtained with a maximum mud deposition area by the model results. This pattern can also be observed in the field data. For 1971-1982 and 1982-1992 the maximum mud deposition is found in the Hollandsch Diep, respectively Hollandsch Diep (W) and Hollandsch Diep (C). Upstream as well as downstream the mud deposition is much lower.

In general, it can be concluded that several observed deposition patterns of sand and mud are also qualitatively reproduced with the morphological sand-mud model. Due to this correspondance between the model results can also be used to give some suggestions and/or explanations for the observed sand-mud patterns:

- The intense mud deposition in the Hollandsch Diep is caused by two interacting factors. On the one hand, the current velocities are low, so mud deposition is possible. On the other hand, the mud concentration is still high due to the absence of mud deposition in the upstream area. Both factors cause a high mud deposition in this section.
- For the Haringvliet the relatively small mud deposition is mainly limited due to the low mud concentration in the water column ('supply limited'). For the upstream areas (Boven-Merwede, Nieuwe Merwede) the relatively small mud deposition is mainly due to the high current velocities ('flow limited'). Consequently, the mud content in the bed is therefore relatively low in both areas, but the reason is completely different.

This suggests that predicting the local mud content by using a local parameter will not be very successful when the supply of mud strongly varies. A local parameter will probably show a lot of scatter, because low mud content in the bed can be found due to high flow velocities (‘flow limited’) as well as low suspended mud concentrations (‘supply limited’).

Several differences between the observed sand-mud patterns and the morphological sand-mud model. Various suggestions can be given for these differences:

- Firstly, the boundary conditions and the geometry are strongly simplified. For example, river discharge variations are not taken into account at the upstream boundary and only a yearly mean value is chosen to be representative. Earlier studies suggest that under these high discharges an enormous amount of sand and mud is transported. Probably these high river discharges cause the sand sedimentation in the Hollandsch Diep and

Haringvliet. Moreover, the width is assumed to be constant in longitudinal direction. Changes in the initial cross-sectional area are translated into changes in initial bed levels only in order to reproduce realistic current velocities along the basin. An application of the sand-mud model in which a more realistic bathymetry and more realistic boundary conditions are applied is recommended for further research.

- Secondly, the sand and mud balances contain a lot of uncertainty. These balances are based on depth soundings, dredging data, bed composition measurements and bifurcation relationships for the distribution of sand and mud transport. The bed composition measurements play a key role in the determination of the deposited and/or eroded sand and mud volume. Often, the mean mud content of the upper ten or twenty centimeters is chosen to be representative for the ratio between the deposed/eroded volume due to mud and the total deposited/eroded volume due to sand and mud. However, it is questionable if this mean mud content is representative, because the mud content can be strongly stratified in the bed. Moreover, the bed composition does not always correspond with the actual deposition conditions. A good example is the Haringvliet. In this area the bed composition is still relatively sandy while the model results suggest only mud deposition.

The model results give also indications for the development in the future when the boundary conditions are not changed. The results suggest that the sand wave will travel in downstream direction and cover the mud layers in the Hollandsch Diep. Furthermore, the mud wave will also travel in downstream direction and the Haringvliet will become more muddy under these conditions. Finally, this area is covered with a sand layer.

The final equilibrium is a ‘river situation’ with a more or less constant cross-sectional area. The mud concentration will be more or less constant along the basin and no mud deposition will take place anymore. The bed composition near the bed surface is completely sandy. More below the bed surface, mud layers which are covered with sand are still present.

5 Conclusions and recommendations

5.1 Conclusions

- Model formulations for a process-based morphological model with a sand and a mud fraction are proposed (Chapter 2). The main extensions to the present morphological models are that the bed level changes depend on both suspended sand and mud exchange at the bed-water interface and bed load transport gradients of sand. Furthermore, the bed composition is time-dependent and non-uniform in horizontal and vertical directions. Important assumptions are that both the settling velocity of mud and the bed roughness are time and space independent.

- The model formulations are implemented in the three-dimensional software package DELFT3D-FLOW (Chapter 3). The bed composition equation is discretized by an FTCS-scheme. This explicit numerical scheme restricts the time step and spatial step for the bed composition computation. Moreover, some artificial diffusion must be added in areas where the physical diffusion is very small to keep the numerical computations stable.

- The morphological behaviour of an estuary in which the tide is eliminated, was analysed (Chapter 4). This situation is qualitatively comparable with the southern area of the Noordelijk Deltabekken (The Netherlands) in which sand and mud was deposited after the construction of the Haringvliet sluices in 1970. The geometry and the boundary conditions were strongly simplified in order to determine governing length scales by an analytical approach.

- The model results showed two deposition areas travelling in the downstream direction (Chapter 4). Initially sand deposition occurs in areas in which the water depth is slightly larger than the equilibrium water depth. The propagation velocity of the sand wave strongly depends on the sediment transport rate and the difference between the actual water depth and the equilibrium water depth. Mud deposition starts at a certain point in the basin. This onset is explained by the critical shear stress for deposition in the deposition formula. Beyond this onset the bed level change due to mud has a characteristic form with a maximum at a certain distance beyond the onset. The form of the mud wave strongly depends on two adaptation length scales for mud: a 'settling length scale' and a 'flow length scale'. The expression for the settling length scale is equal to the well-known adaptation length scale for suspended sand transport, but differs due to another settling velocity. The 'flow length scale' depends on both the actual bed level slope and the critical velocity for mud deposition. This length scale expresses a characteristic distance in which the (depth-averaged) flow velocity becomes two times smaller than the critical (depth-averaged) velocity for deposition.

- Due to the simplified geometry and boundary conditions the computational results could only qualitatively be compared with two sediment balances (1971-1982 and 1982-1992) for several sections in the Noordelijk Deltabekken (Chapter 4). Various morphological characteristics found with the numerical computations (e.g. sand wave, mud wave, maximum mud deposition) are also observed in both or at least one of the

sediment balances. The simplified model set-up and also the determination of the deposited sand and mud volumes in the sediment balances, are causes of several differences between the model results and the field data.

- Specifically for the Haringvliet and Hollandsch Diep, the model results suggest that the high mud deposition rate in the Hollandsch Diep area is caused by two interacting factors (Chapter 4). On the one hand the mud concentration in the water column is relatively high due to the absence of mud in the upstream areas. On the other hand, the flow velocity is relatively low, so mud deposition can occur. For the upstream river branches (Nieuwe Merwede, Boven-Merwede) the relatively low mud deposition compared with the Hollandsch Diep is mainly caused by the high flow velocities. For the downstream area, the relatively low mud deposition is caused by the low mud concentrations in the water column.

- The model results also suggest that predicting the mud content with a local parameter is probably not very successful in areas in which the horizontal mud concentration strongly varies (Chapter 4). Besides the local hydrodynamics, the mud supply from upstream is a very important factor in the development of the local mud content in the bed.

5.2 Recommendations

- The reliability of the model results is (partly) determined by the process formulations used. In particular, the erosion process of a sand-mud bed is not sufficiently understood and the experimental evidence of the erosion formulations used herein are weak. It is recommended to carry out laboratory experiments in order to improve the process formulations for the erosion of sand-mud mixtures.

- The morphological model was applied with a time and space independent roughness coefficient and settling velocity for mud. These parameters however, can strongly vary in time and space. It is recommended to further analyse the model behaviour by applying time and space dependent formulations for both the settling velocity for mud and the bed roughness coefficient.

- The model was applied with time-independent boundary conditions and a very schematic initial bed level profile. Therefore, model results could only qualitatively be compared with field data. It is recommended to apply the model with more realistic boundary conditions and a realistic bathymetry to a part of the Noordelijk Deltabekken in which sand and mud was deposited after the construction of the Haringvliet sluices. For instance, the Nieuwe Merwede can be chosen because in the lower reach the bed consists of both sand and mud layers and a lot of field data exist for this area.

- The model results suggested that predicting the mud content with a local parameter is probably not very successful in areas in which the suspended mud concentration strongly varies in horizontal direction. Non-local effects (e.g. advection of sediment) should also be taken into account. It is recommended to investigate the suggestions given by Wang (1997) for extending the (local) parameter LHEC with non-local effects.

- Mean values for the mud content of the upper ten or twenty centimetres in the bed are often used for validating models and/or determining the sand and mud deposition/erosion rates in sediment balances. However, it is often not known whether

this sample thickness are representative for the actual deposition/erosion rates of the area. It is recommended to estimate the representativeness when bed composition measurements are carried out in the future. A possibility is to determine the bed composition profile in more detail.

Acknowledgement

The author acknowledges the valuable comments and suggestions of dr Z.B. Wang and the help of dr J.A. Roelvink, G. Lesser and R. Bruinsma with the implementation in DELFT3D-FLOW. The comments from dr J.C. Winterwerp, C. Kuijper and prof dr H.J. de Vriend are also highly appreciated. The present part of this project (Part II) was supported by the Technology Foundation STW, applied science division of NWO and the technology programme of the Ministry of Economic Affairs.

6 References

Allersma, E., 1988. *Morfologisch onderzoek Noordelijk Deltabekken (in Dutch)*. Morfologische Modellering deel I: Inleiding en Samenvatting., WL | DELFT HYDRAULICS, Delft.

Armanini, A., 1995. *Non-uniform sediment transport: dynamics of the active layer*. Journal of Hydraulic Research, no. 33, 611-622.

Boudreau, B.P., 1997. *Diagentic models and Their implementation.* Modelling Transport and Reactions in Aquatic Sediments. Springer Verlag, New York.

Kuijper, C., 1995a. *Analysis of field measurements on the Nieuwe Merwede.* Delft Hydraulics (Z743.10), The Netherlands.

Kuijper, C., 1995b. Natural Sand-Mud Beds. Effect of sand on mud properties. Delft Hydraulics (Z743.20), The Netherlands.

Lesser, G., 2000. *Computation of Three-dimensional Suspended Sediment Transport within the DELFT3D-FLOW Module*. WL | DELFT HYDRAULICS (Z2396), IHE Delft (Thesis HE066), The Netherlands.

Stelling, G.S., 1984. *On the construction of computational methods for shallow water flow problems.* Rijkswaterstaat communications, No. 35, The Hague, Rijkswaterstaat, The Netherlands.

Torfs, H., 1995. *Erosion of sand/mud mixtures*. Katholieke Universiteit Leuven, faculteit der Toegepaste Wetenschappen, Departement Burgelijke Bouwkunde, Laboratorium voor Hydraulica, Belgium.

Torfs, H., Mitchener, H., Huysentruyt, H. Toorman, E. 1996. *Settling and consolidation of mud/sand mixtures.* Coastal Engineering, p.27-45.

Van den Boogaard, H.F.P., C. Kuijper, 1995. *Statistical analysis of Mud and Sand Beds*. Prepared for Rijkswaterstaat-RIZA, Delft Hydraulics (Z743.30), The Netherlands.

Van Dreumel, P.F., 1995. *Slib- en zandbeweging in het noordelijk Deltabekken in de periode 1982-1992 (in Dutch)*. Ministerie van Verkeer en Waterstaat, Directie Zuid-Holland, Afdeling Watersysteemkennis, Rotterdam.

Van Ledden, M., 2000. *Sediment segregation in estuaries and tidal lagoons. A literature review.* Delft University of Technology, The Netherlands.

Van Ledden, M., Z.B. Wang, submitted. *A process-based model for sand-mud.* Submitted for INTERCOH-conference 2000, Delft, The Netherlands.

Van Rijn, L.C., 1993. *Principles of sediment transport in rivers, estuaries and coastal seas*. Aqua Publications, The Netherlands.

Venema, L.B., R. ten Have, R.J. de Meijer, B. van Os, J.M.J. Gieske, H.P. Zwanenburg-Nederlof, 1998. *Radiometric Survey of 'Hollandsch Diep'. Part I: Feasibility Study and Radiometric and Geotechnical Characterisation.* Rijksuniversiteit Groningen/TNO. The Netherlands.

Venema, L.B., P. Groen, R.J. de Meijer, B. van Os, J.M.J. Gieske, M. van Wijngaarden, 1999. *Radiometric Survey of 'Hollandsch Diep'. Part II: Mud-sand mapping.* Rijksuniversiteit Groningen/TNO/RWS-RIZA. The Netherlands.

Venema, L.B., J. Limburg, R.J. de Meijer, B. van Os, J.M.J. Gieske, M. van Wijngaarden, 2000. *Radiometric Characterisation of 'Haringvliet' sediment.* Rijksuniversiteit Groningen/TNO/RWS-RIZA. The Netherlands.

Visser, P.J., 2000. *Bodemontwikkeling Rijnsysteem. Een verkenning van omvang, oorzaken, toekomstige ontwikkelingen en mogelijke maatregelen (in Dutch)*. Faculteit Civiele Techniek en Geowetenschappen, Technische Universiteit Delft.

Vreugdenhil, C.B., 1989. *Computational hydraulics. An Introduction.* Springer-Verlag, Berlin, Heidelberg.

Wang, Z.B., 1989. Mathematical modelling of morphological processes in estuaries. Communications on hydraulic and geotechnical engineering, Report 89-1, Faculty of Civil Engineering, Delft University of Technology.

Wang, Z.B., 1996. *Basic theory for predicting bed composition.* Cohesive Sediments (Report 51). Rijkswaterstaat/Delft Hydraulics. The Netherlands.

Wang, Z.B., 1997. *LHEC, A model for predicting mud content in the bed. Pilot application in the Nieuwe Merwede.* Cohesive Sediments (Report 53). Rijkswaterstaat/Delft Hydraulics. The Netherlands.

Winterwerp, J.C., 1999. *On the dynamics of high-concentrated mud suspensions*. Ph.D. thesis, Delft University of Technology, Delft.

A Figures

B Mud wave characteristics

B.1 Onset

The initial bed level is given by:

$$z_b(x) = i_{be}(L_b - x) - h_e - (h_1 - h_e)e^{-\frac{L_b - x}{L_a}} \qquad (.1)$$

z_b = Bed level [m]
i_{be} = Equilibrium bed level [-]
x = Distance from upstream boundary [m]
L_b = Basin length [m]
h_e = Equilibrium water depth [m]
h_1 = Initial water depth at x= L_b [m]
L_a = Adaptation length initial bed level profile [m]

When it is assumed that the water level slope is equal to the equilibrium bed level slope (i_{be}), the initial water depth (h) is given by:

$$h(x) = h_e + (h_1 - h_e)e^{-\frac{L_b - x}{L_a}} \qquad (.2)$$

The discharge per unit width (q) is constant in time and space. The depth-averaged flow velocity is then given by:

$$u(x) = \frac{q}{h_e + (h_1 - h_e)e^{-\frac{L_b - x}{L_a}}} \qquad (.3)$$

in which:
u = Depth-averaged velocity [m/s]
q = Discharge per unit width [m^2/s]

The critical bed shear stress for mud deposition (τ_d) can be translated into a critical velocity for deposition (u_d):

$$u_d = \frac{C}{\sqrt{\mu_c}}\sqrt{\frac{\tau_d}{\rho g}} \qquad (.4)$$

in which:
u_d = Critical depth-averaged velocity for deposition [m/s]
C = Chezy-coefficient [$m^{1/2}$/s]
μ_c = Efficiency factor for currents [-]

τ_d = Critical shear stress for deposition [N/m^2]
ρ = Water density [kg/m^3]
g = Gravitational acceleration [m^2/s]

The efficiency factor for currents (μ_c) is given by:

$$\mu_c = \frac{f_c^{'}}{f_c} \qquad (.5)$$

in which:
$f_c^{'}$ = Grain related friction factor [-]
f_c = Total current-related friction factor [-]

The grain related friction factor ($f_c^{'}$) and the total current-related friction factor (f_c) are given by:

$$f_c^{'} = 0.24\left[\log_{10}\left(\frac{12h}{3d_{90}}\right)\right]^{-2}$$
$$f_c = 0.24\left[\log_{10}\left(\frac{12h}{k_s}\right)\right]^{-2} \qquad (.6)$$

in which:
d_{90} = Grain size 90% [m]
k_s = Roughness height [m]

The roughness height (k_s) is given by the maximum of two expressions:

$$k_s = \frac{h}{100} \quad k_s = \frac{12h}{10^{\frac{C}{18}}} \qquad (.7)$$

When the flow velocity (u) is equal to the critical velocity for deposition (u_d), mud deposition starts. The onset of mud deposition (x_d) is thus given by:

$$u_d = \frac{q}{h_e + (h_1 - h_e)e^{-\frac{L_b - x_d}{L_a}}} \quad \rightarrow \quad \frac{x_d}{L_b} = 1 + \frac{L_a}{L_b}\ln\left(\frac{\frac{q}{u_d h_e} - 1}{\frac{h_1}{h_e} - 1}\right) \qquad (.8)$$

in which:
x_d = Onset of mud deposition [m]
h_d = Critical water depth for mud deposition [m]

At the right-hand side of (B.8) the ratio between the discharge per unit width (q) and the critical velocity for deposition (u_d) is the critical water depth for mud deposition (h_d):

$$h_d = \frac{q}{u_d} \qquad (.9)$$

in which:
h_d = Critical water depth for mud deposition [m]

Thus, the onset of mud deposition (x_d) can be given by:

$$\frac{x_d}{L_b} = 1 + \frac{L_a}{L_b} \ln \left(\frac{\frac{h_d}{h_e} - 1}{\frac{h_1}{h_e} - 1} \right) \qquad (.10)$$

B.2 Mud concentration

When no mud erosion occurs, the depth-averaged mud concentration equation can be given by:

$$q \frac{\partial c_m}{\partial x} = -w_m c_m \left[1 - \frac{u^2}{u_d^2} \right] \qquad (.11)$$

in which:
c_m = Depth-averaged mud concentration [-]
w_m = Settling velocity mud [m/s]

At the onset of mud deposition the flow velocity is equal to the critical velocity for deposition and the water depth is equal to the critical water depth for deposition (see Appendix B.1).

Beyond the onset the water level is assumed to be horizontal. Furthermore, the initial water depth is approximated by a linear initial slope between the onset and the downstream boundary. The flow velocity (u) can then be approximated by:

$$u(x) = \frac{q}{h_d + i_{b0} x} \qquad (.12)$$

in which:
i_{b0} = Initial bed slope [-]
x = Distance to the onset [m]

The initial bed slope (i_{b0}) is given by:

$$i_{b0} = \frac{h_1 - h_d}{L_b - x_d} \qquad (.13)$$

Combining (B.11) and (B.12) the mud concentration along the basin (c_m) can be given as follows:

$$\frac{\partial c_m}{c_m} = -\frac{w_m}{q}\partial x + \frac{w_m}{q u_d^2}\frac{q^2}{\left(\frac{q}{u_d} + i_{b0}x\right)^2}\partial x \qquad (.14)$$

Integrating between x = 0 (i.e. onset) and x = x:

$$\int_0^x \frac{1}{c_m}\partial c_m = -\int_0^x \frac{w_m}{q}\partial x + \int_0^x \frac{w_m}{q u_d^2}\frac{q^2}{\left(\frac{q}{u_d} + i_{b0}x\right)^2}\partial x \qquad (.15)$$

Rewriting gives:

$$\ln c_m = -\frac{w_m}{q}x - \frac{w_m}{q}\frac{1}{i_{b0}u_d^2}\frac{q^2}{\left(\frac{q}{u_d} + i_{b0}x\right)} + c_1 \qquad (.16)$$

Two length scales are introduced:

$$L_m = \frac{q}{w_m} \quad L_d = \frac{q}{i_{b0}u_d} \qquad (.17)$$

Applying these definitions the mud concentration (c_m) is given by:

$$\ln c_m = -\frac{L_d}{L_m}\left[\frac{x}{L_d} + \frac{1}{\left(1 + \frac{x}{L_d}\right)}\right] + c_1 \qquad (.18)$$

The integral coefficient c_1 can be found by applying the boundary concentration ($c_{m,0}$) at x = 0. The coefficient c_1 is equal to:

$$c_1 = \ln c_{m,0} + \frac{L_d}{L_m} \qquad (.19)$$

in which:
$c_{m,0}$ = Mud concentration at boundary x = 0 [-]

Using the integral coefficient the mud concentration (c_m) is given by:

$$\ln c_m(x) = -\frac{L_d}{L_m}\left[\frac{x}{L_d} + \frac{1}{\left(1+\frac{x}{L_d}\right)} - 1\right] + \ln c_{m,0} \qquad (.20)$$

$$c_m(x) = c_{m,0} e^{-\frac{1}{L_m}\frac{x^2}{(L_d+x)}}$$

The mud deposition rate (D) is given by:

$$D(x) = w_m c_m \left[1 - \frac{u^2}{u_d^2}\right] \qquad (.21)$$

in which:
D = Mud deposition rate [m/s]

By using the expressions for the flow velocity (u) and the mud concentration (c_m) the deposition rate (D) is given by:

$$D = w_m c_{m,0} e^{-\frac{1}{L_m}\frac{x^2}{(L_d+x)}}\left[1 - \frac{1}{\left(1+\frac{x}{L_d}\right)^2}\right] \qquad (.22)$$

B.3 Maximum mud deposition

The maximum mud deposition occurs when the derivative of the mud deposition rate (D) to x is equal to zero. By using the expression for the deposition (B.21):

$$D(x) = w_m c_{m,0} e^{f(x)} g(x) \quad f(x) = -\frac{1}{L_m}\frac{x^2}{(L_d+x)} \quad g(x) = \left[1 - \frac{1}{\left(1+\frac{x}{L_d}\right)^2}\right] \qquad (.23)$$

$$\frac{dD}{dx} = 0 \quad \rightarrow \quad f'(x)g(x) + g'(x) = 0$$

The derivative of function f(x) is given by:

$$f(x) = -\frac{1}{L_m}\frac{x^2}{(L_d + x)} \rightarrow f'(x) = -\frac{1}{L_m}\frac{\frac{x}{L_d}\left(\frac{x}{L_d}+2\right)}{\left(1+\frac{x}{L_d}\right)^2} \qquad (.24)$$

The derivative of function g(x) is given by:

$$g(x) = 1 - \frac{1}{\left(1+\frac{x}{L_d}\right)^2} \rightarrow g'(x) = \frac{\frac{2}{L_d}}{\left(1+\frac{x}{L_d}\right)^3} \qquad (.25)$$

By using the expression for f'(x) in (B.23) and g'(x) in (B.24) the derivative of the mud deposition rate (D) to x is then given by:

$$\frac{dD}{dx} = f'(x)g(x) + g'(x)$$

$$\frac{dD}{dx} = -\frac{1}{L_m}\frac{\frac{x}{L_d}\left[\frac{x}{L_d}+2\right]}{\left[1+\frac{x}{L_d}\right]^2}\left[1-\frac{1}{\left(1+\frac{x}{L_d}\right)^2}\right] + \frac{\frac{2}{L_d}}{\left(1+\frac{x}{L_d}\right)^3} = 0 \qquad (.26)$$

$$\frac{dD}{dx} = -\frac{1}{L_m}\frac{\frac{x}{L_d}\left[\frac{x}{L_d}+2\right]\left[\left(1+\frac{x}{L_d}\right)^2-1\right]}{\left[1+\frac{x}{L_d}\right]^4} + \frac{\frac{2}{L_d}}{\left(1+\frac{x}{L_d}\right)^3} = 0$$

This can be further reduced to:

$$\frac{dD}{dx} = -\frac{1}{L_m}\frac{\frac{x}{L_d}\left[\frac{x}{L_d}+2\right]\left[\left(1+\frac{x}{L_d}\right)^2-1\right] - \frac{2L_m}{L_d}\left(1+\frac{x}{L_d}\right)}{\left[1+\frac{x}{L_d}\right]^4} = 0 \qquad (.27)$$

$$\frac{dD}{dx} = \left(\frac{x}{L_d}\right)^4 + 4\left(\frac{x}{L_d}\right)^3 + 4\left(\frac{x}{L_d}\right)^2 - \frac{2L_m}{L_d}\left(\frac{x}{L_d}\right) - \frac{2L_m}{L_d} = 0$$

This is a fourth-order polynom for x/L_d. There are no analytical solutions for this equation. For $x/L_d << 1$ the first term is very small. By ignoring the first term in (B.26), the remaining third order polynom has the following solutions:

$$\frac{dD}{dx} = 4\left(\frac{x}{L_d}\right)^3 + 4\left(\frac{x}{L_d}\right)^2 - \frac{2L_m}{L_d}\left(\frac{x}{L_d}\right) - \frac{2L_m}{L_d} = 0$$
$$x_1 = -L_d, \quad x_2 = -\frac{1}{2}\sqrt{2}\sqrt{L_d L_m}, \quad x_3 = +\frac{1}{2}\sqrt{2}\sqrt{L_d L_m} \qquad (.28)$$

Only the third solution (x_3) is realistic, because we are only interested in solutions downstream from the onset ($x > 0$). It can be seen that the distance of the maximum deposition rate beyond the onset depends on both length scales (L_d and L_m).